Journal of Molecular Structure 1298 (2024) 137078

Contents lists available at ScienceDirect

Journal of Molecular Structure

journal homepage: www.elsevier.com/locate/molstr

Monohalogenated methyl- and methoxy-benzoic acids: A combined experimental and quantum chemical theoretical study on their structure, vibrational analysis and molecular parameters

Sreenivas Boda [a], L. Ravindranath [b], K. Srishailam [c], G. Ramesh [d], Jai Kishan Ojha [e], B. Venkatram Reddy [a,*]

[a] Department of Physics, Kakatiya University, Warangal 506009, Telangana, India
[b] Department of Physics, Malla Reddy Engineering College (A), Hyderabad 500100, Telangana, India
[c] Department of Physics, School of Sciences, SR University, Warangal 506371, Telangana, India
[d] Department of Physics, University P.G College (Satavahana University), Godavarikhani 505209, Telangana, India
[e] Department of Physics, Government Degree College, Luxettipet 504215, Telangana, India

ARTICLE INFO

Keywords:
Halogenated methyl- and methoxy-benzoic acids
DFT
HOMO-LUMO
Reactive descriptors
NLO
NBO

ABSTRACT

In this paper, the molecules 3-fluoro-2-methylbenzoic acid; 3-chloro-2-methoxybenzoic acid; and 3-bromo-2-methylbenzoic were investigated using experimental and quantum chemical theoretical approach for vibrational and electronic properties from the optimized structure. Becke three parameter Lee–Yang–Parr density functionals along with 6-311++G(d,p) basis set were employed to compute their geometric optimization, fundamental frequencies and molecular parameters. The detected FT-IR and FT-Raman spectra were compared with their simulated spectra and the rms error between the detected and simulated vibrational frequencies was found at 6.17, 7.22 and 6.76 cm^{-1} for FMA, CMA and BMA, respectively. All the vibrational fundamentals were assigned unequivocally using potential energy distribution (PED) obtained in the computations. ^{1}H and ^{13}C NMR chemical shifts were evaluated by integrating the gauge-independent atomic orbital (GIAO) method with DFT and compared with corresponding experimental values. TD-DFT approach was followed to compare the simulated absorption maxima (λ_{max}) in DMSO-d_6 solvent with observed values and interpreted in terms of HOMO and LUMO. The global reactive descriptors were estimated from the associated energies of HOMO and LUMO which describe the reactivity and stability of the molecules. Molecular electrostatic potential (MEP) surface has been determined using the charge density distributions to demonstrate electrophilic and nucleophilic nature of the molecules. DFT computations also ascertained the applicability of the titled molecules as NLO materials from the computed values of dipole moment and hyperpolarizability. Thermodynamic parameters and rotational constants were also evaluated employing rigid rotor harmonic oscillator approximation. Natural bond orbital (NBO) analysis confirmed the charge delocalization due to intra-molecular interactions.

1. Introduction

Benzoic acid and its derivatives are being attracted by growing researchers for investigation due to their biological activity, which occur widely in plants and animals tissues. They are constituents of vitamin B-complex and lenticular pigments present in the eye lenses of humans and in certain diurnal animals [1,2]. They are also widely used in the manufacture of pharmaceuticals and miticides as contrast media in urology, cholocystrographic investigations, etc. They also find usage in dyes, curing tobacco, fruit juices preservation, a large variety of esters as a mordant in cloth printing and as a reference standard in volumetric analysis. They are also used as a protective drug against UV radiation in the diagnosis of gastrointestinal disorders and therapeutically in fibrotic skin disorders [3]. The derivatives of benzoic acids play a vital role in minimising the population of mosquitoes [4]. They are also used as important inhibitors for bacteria growth [5] and affect the catalytic activity of various enzymes [6]. Organic materials like 4-aminobenzoic acid and p-chlorobenzoic acid have been used in sun care products as they exhibit excellent UV ray absorption ability [7]. The compound; 2,3,5-tri-iodobenzoic acid was studied for its FTIR and Laser Raman spectra

* Corresponding author.
E-mail address: bvreddy67@yahoo.com (B.V. Reddy).

https://doi.org/10.1016/j.molstruc.2023.137078
Received 17 September 2023; Received in revised form 12 November 2023; Accepted 13 November 2023
Available online 15 November 2023

and the vibrational analysis was made by Chapman et al. [8]. Sundaraganesn et al. [9,10] studied the structure and vibrational analysis of 2-chlorobenzoic acid and 4-methoxy-2-methylbenzoic acid using vibrational spectra and DFT methods along with NLO behaviour and HOMO-LUMO analysis for the later. Gu et al. [11] studied the solubility of 3-bromo-2-methylbenzoic acid in different solvents at different temperatures. 3-bromo-2-methylbenzoic acid has been widely used in pharmaceuticals as important drug intermediate in the synthesis of anticancer drug. It is a good model for investigating the solubility behaviour of pharmaceutics. A.S. Batsanov [12] reported the structure of 3-fluoro-4-methylbenzoic acid using XRD data. Inspiring from the established importance of benzoic acid and its derivatives as biologically active substances, we have investigated some derivatives of benzoic acids [13–18] in our laboratory and reported results on the structure and molecular characteristics. Pryidine-3-carboxylic acid [13] was studied for its barrier potentials, both monomeric and dimeric structure along with hydrogen bond interactions, vibrational analysis and its molecular characteristics using experimental and DFT methods. Some bipyridine-dicarboxylic acids [14] were investigated using experimental; and DFT and IVP theoretical methods to determine their barrier potentials, structure, and force field; and to make vibrational analysis. The molecules, 3-methyl-4-nitrobenzoic acid [15]; and 2,3-; 2,4- and 3,4-pyridine-dicarboxylic acids [16] were investigated by recording their FTIR and FT-Raman spectra and employing IVP and DFT methods for vibrational analysis and force field calculations along with NLO behaviour, HOMO-LUMO energies and thermodynamic parameters. Vibrational spectral analysis of 3,6-dichloropyridazine-4-carboxylic acid [17] was studied using FT-IR and FT-Raman spectroscopic techniques in conjunction with DFT to determine the molecular structure, NLO effect, NBO analysis; ^{13}C and ^{1}H NMR chemical shifts and global reactive descriptors. 4-methyl-3-nitrobenzoic acid [18] was studied for its structure, vibrational assignments and NLO behaviour employing vibrational spectra and DFT method. Pramanik et al. [19] have investigated five benzoic acid derivatives, viz, 2-fluoro-4-hydroxymethyl benzoic acid, 4-chloro-3-nitrobenzoic acid, 5-bromo-2-methylbenzoic acid, 4-bromo-2-nitrobenzoic acid and 4-chloro-2-iodobenzoic acid and reported their structure using PXRD and DFT along with molecular electrostatic surface potential (MESP) and HOMO-LUMO energies. Liu et al. [20] synthesized and characterised the helical architecture of 1,2,3,4-tetra-(4-pyridyl)-butane and 3-bromo-2-methyl benzoic acid using experimental and theoretical method and also studied hydrogen and halogen bonding due to intra- and inter-molecular interactions.

So, the survey of literature [1–20] reveals that the chosen molecules viz, 3-fluoro-2-methylbenzoic acid (FMA); 3-chloro-2-methoxybenzoic acid (CMA); and 3-bromo-2-methylbenzoic acid (BMA) are not paid much attention so far to report their optimized structure, complete vibrational analysis and other electronic and molecular parameters approaching the quantum chemical computations. Hence, this study was undertaken to determine the optimized structure along with ^{1}H and ^{13}C NMR chemical shifts, global reactivity descriptors using frontier molecular orbital (FMO) analysis and electronic absorption maxima, NLO behaviour by evaluating dipole moment and first-order hyperpolarizability, and molecular electrostatic potential (MEP) to demonstrate the electrophilic and nucleophilic sites; and vibrational assignments of FTIR and FT-Raman spectra using quantum chemical density functional theory (DFT) and the results are presented in this paper.

2. Materials and methods

2.1. Experimental details

The test compounds under investigation viz, 3-fluoro-2-methylbenzoic acid (FMA); 3-chloro-2-methoxybenzoic acid (CMA); and 3-bromo-2-methylbenzoiuc (BMA) were procured with a stated purity of 98–99 % from TCI Chemical Company, Japan and used for spectral measurement without extra purification. The FT-IR spectra of these molecules were recorded in the spectral range 4000–450 cm^{-1} employing the KBr optics method using BRUCKER IFS 66 V Spectrometer having resolution of 2 cm^{-1} and scanning speed of 30 cm^{-1}/min. The FT-Raman spectra were obtained in Stokes region of 4000–50 cm^{-1} by FRA-106 Raman Spectrometer excited by Nd:YAG laser source of 1064 nm wavelength operating at 200 mW power and with a spectral width 2 cm^{-1}. ^{1}H and ^{13}C chemical shifts were determined in ppm from NMR spectra which was recorded in DMSO-d_6 environment on Bruker's Avance III HD Spectrometer at 500 MHz with spectral resolution of 10 KHz at room temperature. The UV–visible spectra of these molecules have been recorded in DMSO-d_6 solvent in the range 200–400 nm at room temperature using Jasco UV–visible Spectrophotometer.

2.2. Computational details

All the required quantum chemical calculations have been performed using density functional theory (DFT) employing exchange-correlation functional B3LYP [21] with the enlarged basis set 6-311++G(d,p) [22] in gas phase with the help of Gaussian 09 W program [23].

The necessary prerequisite to initiate the computations for structural, vibrational characteristics and molecular parameters utilizing the quantum chemical approach is the accessibility of trustworthy structure contains bond distances, bond angles and dihedral angles for any molecular systems. If the experimental structure is not available, it is a considerable practice to use the structural data of a related molecule or to fetch the appropriate data from Gauss View 5.0 [24] source to get a basic structure of the molecule for geometry optimization progression in DFT computations. So, the title compounds were optimized without any symmetry constraints and computed ground state geometrical parameters using the experimental structure parameter values available in literature for 3-fluoro-4-methylbenzoic acid [12] and 3-bromo-2-methylbenzoic acid [20]; and also drawing considerable help from Gauss View [24]. The molecular optimization yielded C_1 point group symmetry for all the three molecules under study.

Utilizing the C_1 symmetry as equilibrium structure; the force constants, harmonic vibrational wave numbers, dipole moment and its derivatives along with other molecular parameters were calculated. The equilibrium geometry and the associated force constants created the preliminary data for all subsequent computations. The cartesian force constants were transformed into a non-redundant set of natural internal coordinates following the method suggested by Fogarasi et al. [25]. Further, the force constants so derived were scaled by refining them employing least-squares method proposed by Pulay et al. [26] using MOLVIB 7.0 program [27,28] so that the good possible fit between the observed and calculated wave numbers is achieved. The eigen vectors and potential energy distribution (PED) obtained in the process were used to make vibrational assignments of all the fundamental frequencies of the three test molecules. The procedure put forwarded by Latajka et al. [29] was used for computing the relative infrared intensities, whereas the relative Raman scattering intensities were evaluated by approaching the method suggested by Kereztury et al. [30,31]. The NMR ^{1}H and ^{13}C chemical shift values have been computed with GIAO (Gauge-independent atomic orbital) approach [32] integrating with B3LYP/6-311++G(d,p) method. The UV–visible absorption spectra of the title compounds were simulated by TD-DFT (Time-dependent Density Functional Theory) method [33] with exchange correlational functional B3LYP and 6-311++G(d,p) basis set in DMSO-d_6 solvent. The polarisable continuum model (PCM) in association with the integral equation formalism (IEF) variant proposed by Scalamani and Frisch [34], which was incorporated into Gaussian 09 W program was used to take care from the solvent effects while this spectra is being simulated. The computed values of absorption maxima were compared with the associated detected values in electronic spectra. The global reactive descriptors like electron affinity, ionisation potential, global hardness

and softness, chemical potential and electrophilicity power were evaluated from the frontier molecular orbitals, which were visualized using Gauss View 5.0 software [24]. The dipole moment, molecular polarizability and first order hyperpolarizability were computed to study the non-liner optical (NLO) behaviour of the molecules following the Buckingham's procedure [35] employing finite field approach using the same level of DFT. Natural bond orbital (NBO) analysis was made using NBO 3.1 program [36] by integrating into the Gaussian 09 W program to study the electron delocalization caused due to the various second order molecular interactions between the occupied and unoccupied orbitals of different subsystems of a molecule. The reactive sites of the title compounds were evaluated by using the molecular electrostatic potential (MEP) surface obtained from the DFT computations. Thermodynamic parameters and rotational constants were also computed with the same level of theory.

3. Results and discussion

3.1. Optimized molecular geometry and hydrogen bonding

The optimized molecular geometry of the three molecules was acquired by solving iterative self-consistent field equations without using any equilibrium constraints and observed that there was no negative or imaginary frequency in the computations done at DFT/B3LYP/6-311++G(d,p) level of theory [21,22] using Gaussian 09 W program [23]. The geometry optimization substantiates the stability of the structure with the lowest energy -1469.072×10^3, -2612.673×10^3 and -7965.265×10^3 kJ mol^{-1} for FMA, CMA and BMA, respectively assuming C_1 point group symmetry. The optimized structures along with numbering of atoms of these molecules are illustrated in Fig. 1.

The values of bond lengths, bond angles and dihedral angles along with the experimental values available in literature for 3-fluoro-4-methylbenzoic acid [12] and 3-bromo-2-methylbenzoic acid [20] are collected in Table 1. This table also comprises the parameters involved in intra-molecular hydrogen bond interactions present in the three molecules. It can be witnessed from Table 1 that the theoretical structure parameters for FMA, CMA and BMA are comparable with the experimental literature values [12,20]. As an example, the average value of C—C bond length that connects the acid group with the benzene ring in three molecules is computed at 1.50 Å, which are very near to the experimental value at 1.481 Å [12] and 1.509 Å [20]. Similarly, the length of inter-link C—C bond between benzene ring and methyl group in FMA and BMA is calculated as 1.508 and 1.509 Å, respectively, which are very close to the corresponding experimental value with 1.505 Å [12] and 1.527 Å [20]. The mean bond length of C—C bonds of benzene ring in the three molecules FMA, CMA and BMA was found as 1.396, 1.396 and 1.398 Å; and can be observed that they are very near to the average experimental value at 1.390 Å [12] and 1.382 Å [20]. Also, we can observe that the bond length of C—F and C—Br in FMA and BMA is estimated at 1.359 Å and 1.928 Å, which coincides with the observed value 1.359 Å [12] and 1.875 Å [20].

The mean distance of bonds C7-O13 and C7-O14 carboxylic moiety was computed as 1.207 and 1.353 Å, which is very close association with the available observed values at 1.235 and 1.307 Å; and 1.210 and 1.293 Å of the related molecules [12,20]. The mean bond angle (C—C—C) of benzene ring is computed at 119.99° for the three molecules and it is in better agreement with experimental literature value 120° [12] and 119.98° [20]. The average bond angle (C—C—H) of benzene with methyl group moiety is obtained at 110.99° and 110.80° for BMA and FMA molecules, which are found to be very close to the observed literature value of 111.9°. The mean bond angle of C2-C1-C7, C1-C7-O13 and C1-C7-O14 corresponding to the aromatic nucleus and substituent acid group is found at 123.07°, 124.00° and 114.81°, respectively in the three molecules and can be observed that it is closely associated with corresponding experimental literature value at 120.18°, 120.58° and 114.91°; and 123.3°, 124.1° and 11.7° of related molecules [12,20]. It can be evidenced from Table 1 for dihedral angles of methyl and methoxy group of the respective molecules that the hydrogen atoms are distributed as in-plane, below-plane and above plane of the aromatic nucleus.

The structures depicted in Fig. 1, which are optimized at DFT/B3LYP/6-311++G(d,p) level of theory, reveal the existence of intramolecular interactions in the three molecules under study. Each of the three molecules forms two hydrogen bonds, one with oxygen atom and the other with halogen atom. They are existed as (C—H…O) and (C—H…F/Cl/Br) and are found to be 2.297 and 2.293 Å in FMA; 2.427 and 2.757 Å in CMA, 2.457 and 2.686 Å in BMA, respectively. These values are well within the range to form bond for hydrogen interaction. The bond angles corresponding to the hydrogen bonding are also shown in Table 1. All the theoretical investigations were made in the gaseous state, whereas the experimental data were obtained from the solid state and hence, the calculated values have small deviations from the experimental literature values of the related molecules [12,20].

3.2. Vibrational analysis

Vibrational modes were investigated by harmonic wavenumber computations carried out for the associated energy optimized molecular structure of the chosen molecules which assumed C_1 point group symmetry as discussed in the previous section. The vibrational assignments were made by comparing with the available literature for the related molecules and also based on the DFT computation results.

Both molecules, FMA and BMA, are composed of 18 atoms each

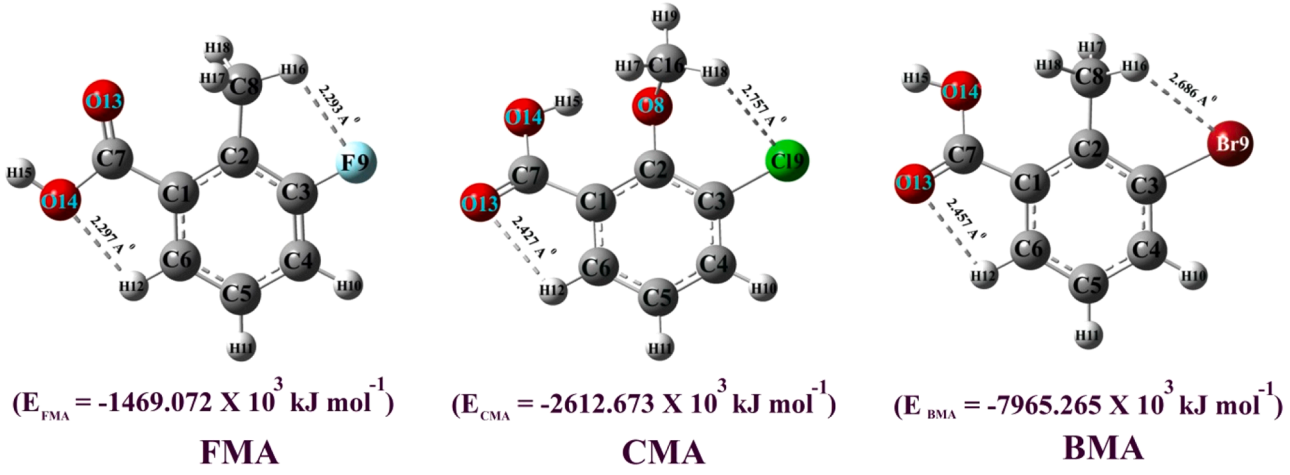

Fig. 1. Optimized molecular structure of FMA, CMA and BMA along with numbering of atoms and minimum energy.

Table 1
Experimental and DFT/B3LYP/6-311++ G(d,p) optimized geometric parameters of FMA, CMA and BMA.

Geometric parameter	Calculated Value			Experimental Value	
	FMA	CMA	BMA	Ref. [12]	Ref. [20]
Bond lengths (in Å)					
C1-C2	1.416	1.407	1.416	1.395	1.379
C2-C3	1.395	1.400	1.404	1.379	1.390
C3-C4	1.385	1.390	1.392	1.389	1.390
C4-C5	1.391	1.392	1.390	1.396	1.373
C5-C6	1.388	1.388	1.386	1.393	1.360
C6-C1	1.403	1.399	1.400	1.389	1.400
C1-C7	1.489	1.514	1.497	1.481	1.509
C7-O13	1.210	1.204	1.209	1.235	1.210
C7-O14	1.361	1.344	1.356	1.307	1.293
O14-H15	0.968	0.977	0.969	0.920	*
C3-F9/Cl9/Br9	1.359	1.753	1.928	1.359	1.875
C4-H10	1.083	1.083	1.082	*	*
C5-H11	1.083	1.083	1.083	*	*
C6-H12	1.080	1.082	1.082	*	*
C2-C8	1.508	–	1.509	1.505	1.527
C8-H16	1.088	–	1.089	*	*
C8-H17	1.091	–	1.094	*	*
C8-H18	1.091	–	1.087	*	*
C2-O8	–	1.380	–	*	*
O8-C16	–	1.448	–	*	*
C16-H17	–	1.093	–	*	*
C16-H18	–	1.090	–	*	*
C16-H19	–	1.088	–	*	*
Bond angle (in°)					
C1-C2-C3	115.68	119.34	115.83	117.86	119.1
C2-C3-C4	124.38	120.85	123.17	124.15	120.0
C3-C4-C5	118.68	119.66	119.52	116.56	120.4
C4-C5-C6	119.56	120.05	119.38	121.15	119.9
C5-C6-C1	120.88	120.88	120.80	120.10	120.5
C6-C1-C2	120.81	119.18	121.25	120.18	120.0
C1-C2-C8	124.84	–	123.15	121.47	*
C3-C2-C8	119.48	–	120.99	121.97	*
C2-C8-H16	110.35	–	110.35	110.8	*
C2-C8-H17	111.03	–	110.94	112.2	*
C2-C8-H18	111.03	–	111.67	112.8	*
C2-C3-F9/Cl9/Br9	118.64	120.11	120.80	117.88	122.2
C4-C3-F9/Cl9/Br9	116.97	119.02	116.02	117.96	117.8
C3-C4-H10	119.22	119.29	119.79	118.9	*
C5-C4-H10	122.09	121.05	120.69	120.10	*
C4-C5-H11	120.11	119.68	120.06	123.0	*
C6-C5-H11	120.33	120.27	120.56	115.8	*
C5-C6-H12	120.11	121.38	120.90	120.3	*
C1-C6-H12	119.01	117.74	118.29	*	*
C6-C1-C7	118.87	116.53	114.13	119.35	116.7
C2-C1-C7	120.31	124.28	124.62	120.18	123.3
C1-C7-O13	126.29	121.67	124.05	120.58	124.1
C1-C7-O14	112.74	117.32	114.36	114.91	111.7
C7-O14-H15	106.25	109.25	106.43	111.01	*
O13-C7-O14	120.97	121.00	121.52	121.65	124.1
C2-O8-C16	–	115.90	–	*	*
O8-C16-H17	–	110.07	–	*	*
O8-C16-H18	–	110.59	–	*	*
O8-C16-H19	–	105.75	–	*	*
Dihedral angle (in°)					
C1-C2-C3-C4	−0.003	−1.786	−1.273	−1.15	*
C2-C3-C4-C5	−0.001	−0.555	−0.371	−0.555	*
C3-C4-C5-C6	0.001	0.557	0.834	0.6	*
C4-C5-C6-C1	0.000	0.422	0.406	1.0	*
C5-C6-C1-C2	−0.003	−0.814	−2.157	−0.3	*
C6-C1-C2-C3	0.005	1.895	2.507	0.8	*
C6-C1-C2-C8	179.99	–	175.85	179.20	*
C4-C3-C2-C8	−179.99	–	−177.12	−178.59	*
C3-C2-C8-H16	0.029	–	27.725	0.2	*
C3-C2-C8-H17	−121.03	–	−91.553	*	*
C3-C2-C8-H18	121.10	–	148.90	*	*
C1-C2-C8-H16	−179.97	–	−150.54	*	*
C1-C2-C8-H17	58.970	–	90.174	*	*
C1-C2-C8-H18	58.900	–	29.373	*	*
C1-C2-C3-F9/Cl9/Br9	180.00	176.73	178.31	*	*
C5-C4-C3-F9/Cl9/Br9	−180.00	−177.98	−179.97	*	*
C2-C3-C4-H10	180.00	179.94	179.99	*	*
C6-C5-C4-H10	−180.00	−178.82	−179.54	*	*

(*continued on next page*)

Table 1 (*continued*)

Geometric parameter	Calculated Value			Experimental Value	
	FMA	CMA	BMA	Ref. [12]	Ref. [20]
C3-C4-C5-H11	180.00	179.90	179.37	*	*
C1-C6-C5-H11	−180.00	−179.76	−179.38	*	*
C4-C5-C6-H12	180.00	179.36	179.97	*	*
C2-C1-C6-H12	180.00	179.40	178.26	*	*
C5-C6-C1-C7	179.99	178.28	177.46	*	*
C3-C2-C1-C7	−179.99	−177.13	−177.07	*	*
C6-C1-C7-O13	179.96	12.468	25.914	*	*
C2-C1-C7-O13	−0.031	−168.48	−154.48	*	*
C6-C1-C7-O14	−0.034	−166.12	−151.19	*	*
C2-C1-C7-O14	179.97	12.930	28.409	*	*
C1-C7-O14-H15	180.00	177.213	178.13	*	*
O13-C7-O14-H15	0.002	1.38	0.946	*	*
C6-C1-C2-O8	–	178.68	–	*	*
C4-C3-C2-O8	–	−178.55	–	*	*
C3-C2-O8-C16	–	−79.145	–	*	*
C1-C2-O8-C16	–	104.11	–	*	*
C2-O8-C16-H17	–	−64.434	–	*	*
C2-O8-C16-H18	–	62.701	–	*	*
C2-O8-C16-H19	–	177.11	–	*	*

Bifurcated intra-molecular hydrogen bond geometry (bond length in Å; and bond angles in degrees) for FMA, CMA and BMA.

Molecule	DH•••A	D—H	H•••A	D•••A	∠D—H•••A
FMA	C6-H12•••O14	1.081	2.297	2.393	99.36
	C8-H16•••F9	1.088	2.293	2.791	105.66
CMA	C6-H12•••O13	1.082	2.427	2.791	97.97
	C16-H18•••Cl9	1.089	2.757	3.367	115.14
BMA	C6-H12•••O13	1.082	2.457	2.806	97.16
	C8-H16•••Br9	1.089	2.686	3.190	107.73

–: Not relevant; *: Not available.

which set into 48 fundamental vibrations, whereas the molecule CMA is constituted with 19 atoms which resulted into 51 vibrational modes. All the fundamental vibrations of the three molecules having C_1 symmetry fit into a-species and are active in both infrared and Raman spectra under this symmetry.

Observed infrared and Raman frequencies; the associated unscaled and scaled frequencies with DFT; computed infrared and Raman intensities; vibrational assignments along with PED; and mode of vibration for FMA, CMA and BMA are depicted in Tables 2–4, respectively. Vibrational modes instigating from benzene ring are expressed in Wilson's notation [37] in these tables. Both experimental and DFT simulated FT-IR spectra are compared in Figs. 2, 4 and 6, whereas for FT-Raman counterparts are compared in Figs. 3, 5 and 7 for FMA, CMA and BMA, respectively. During the DFT computations, it was found that neither negative nor imaginary wavenumber was present in the simulated vibrational frequencies which testify the correctness of the optimized molecular geometry in the ground state that was identified at the global minimum potential energy for the three molecules. It is established fact that the DFT computations systematically overestimate the vibrational frequencies. Thus, these errors are corrected by making anharmonic corrections unambiguously by employing the scaling of the calculated vibrational frequencies [26] and using MOLVIB program designed by Sundius [27,28]. The rms error between the experimental and scaled frequencies is estimated at 6.17, 7.22 and 6.76 cm^{-1} for FMA, CMA and BMA, respectively. It can be understood from the rms error and the comparison of experimental and simulated vibrational spectra shown in Figs. 2–7 that the observed frequencies are in very close vicinity of the corresponding calculated frequencies. This established the correctness of the structure optimized for the molecules under study. The vibrational assignments demonstrated in Tables 2–4 reveal that there is considerable mixing of the ring vibrations and also between those of ring and substituents. The analysis of the vibrations is very intricate since the studied molecules possessed the low symmetry. Particularly, substituent and out-of plane vibrations are very tedious to attribute due to the mixing of other vibrational character. In spite of this complexity, the vibrational assignments of all the fundamentals for the three molecules are suggested unequivocally based on the potential energy distribution (PED) obtained in the DFT computations and the assignments made earlier for related molecules [38–43]. The assignments of fundamental vibrations suggested in Tables 2–4 are easy to understand and hence the discussion is confined to the substituent vibrations only.

3.2.1. *C-X vibrations (X = F, Cl and Br)*

The vibrations associated with C-X (*X* = F, Cl and Br in FMA, CMA and BMA, respectively) bond are identified as ν(CX) (stretching), β(CX) (in-plane bending) and π(CX) (out-of-plane bending) and represented as modes 7b, 18b and 17b in Wilson's notation [37], respectively. The strong absorptions at 890, 372R* (* R indicates Raman shift) and 289R cm^{-1} with associated calculated frequencies near 892, 376 and 287 cm^{-1} having PED to the extent of 21 %, 13 % and 26 % from C-X stretching character are assigned as mode 7b in FMA, CMA and BMA, respectively. Similarly, weak band in Raman scattering at 293 cm^{-1} and moderately strong Raman line near 260 cm^{-1} along with simulated frequencies 288 and 265 cm^{-1} consisting 31 % and 22 % PED from C-X in-plane bending character in CMA and BMA, respectively, whereas the calculated frequency at 324 cm^{-1} with PED to the extent of 66 % in FMA are ascribed to mode 18b. Further, the Raman shifts at 248 and 206 cm^{-1} in FMA and CMA, whereas the calculated frequency near 122 cm^{-1} is attributed to C-X out-of-plane bending mode 17b in the three molecules, respectively. The assignments of various frequencies now suggested for C-X vibrations in the three molecules are in good agreement with those made in case of mono-halogenated anisoles [38]; nitrotoluenes, dimethylanilines and some substituted methylbenzenes [39]; and 5-fluoro- and 5-chloro-salicyclic acid [40].

3.2.2. *Methyl and methoxy group vibrations*

The hydrogen atom at 2nd position in benzene ring is substituted with methyl group in the molecules FMA and BMA; and with methoxy group in CMA molecule. There are nine vibrations associated with the methyl group in FMA and BMA, whereas methoxy group in CMA comprises twelve vibrations. The three stretching vibrations are denoted as $\nu_s(CH_3)$, $\nu_{as}(CH_3)_{ip}$, and $\nu_{as}(CH_3)_{op}$; three deformations viz, $\delta_s(CH_3)$, $\delta_{as}(CH_3)_{ip}$ and $\delta_{as}(CH_3)_{op}$; two rocking vibrations $\gamma(CH_3)_{ip}$ and $\gamma(CH_3)_{op}$;

Table 2
Observed, calculated frequencies (in cm^{-1}) with DFT/6-311++G(d,p) and vibrational assignment of FMA.

S. no.	Obs. freq. (cm^{-1})		Cal. freq. (cm^{-1})		Intensity[a]		Vibrational assignment[b]	Mode identification[c]
	IR	Raman	Un-scaled	Scaled	IR (I_i)	Raman (S_i)		
(i) Vibrations of aromatic unit								
1	–	3074	3224	3070	0.37	47.42	99(2)	ν(CH)2
2	3052	–	3201	3048	0.72	82.05	99(20b)	ν(CH)20b
3	3010	–	3185	3032	1.31	35.68	99(7a)	ν(CH)7a
4		1621	1647	1624	2.16	17.87	66(8b)+15(18a)+10(6b)	ν(CC)8b
5	1608	–	1612	1599	9.06	15.56	62(8a)+13(18a)+11(6b)	ν(CC)8a
6	–	1490	1499	1489	14.55	0.35	43(3)+32(19b)+17[$\delta_{as}(CH_3)_{ip}$]	ν(CC)19b
7	1463	–	1490	1468	16.33	2.08	38(19a)+27(3)	ν(CC)19a
8	1312	1320	1328	1315	3.84	1.85	79(14)	ν(CC)14
9	–	1259	1262	1259	34.05	13.34	34(7b)+24(3)+21(14)+10(12)	β(CH)3
10	–	1230	1234	1232	37.41	8.91	32(14)+22(3)+10[δ(OH)]+10(20a)	$\nu(CC_\alpha)$20a
11	–	–	1211	1204	14.97	1.36	22(13)+21(12)+20(9b)+14(14)	$\nu(CCH_3)$13
12	1175	1170	1184	1177	2.00	6.51	50(9b)+21(14)+13(13)	β(CH)9b
13	1074	1080	1092	1081	7.36	14.27	46(1)+23(18a)+11(12)	β(CH)18a
14	–	978	985	975	0.01	0.02	73(5)+26(16a)	π(CH)5
15	913	–	930	915	0.12	0.01	78(17a)+19(16b)	π(CH)17a
16	890	893	894	892	14.28	0.55	23(19b)+21(7b)+16(12)+12[$\nu(C_\alpha$—O)]+11[$\gamma(CH_3)_{ip}$]	ν(CF)7b
17	814	–	825	816	1.09	0.69	56(12)+23(13)	β(CCC)12
18	–	–	823	809	0.09	0.09	34(11)+24[$\omega(C_\alpha$═O)]+21(4)+13(10a)	π(CH)11
19	–	–	708	700	0.64	0.06	61(4)+10[$\omega(C_\alpha$═O)]	τ(CCCC)4
20	620	617	619	613	2.13	3.51	31(12)+19[$\delta(C_\alpha$═O)]+14[$\gamma(C_\alpha$—O)]+13(1)	ν(CC)1
21	–	550	569	553	1.38	1.76	26(6b)+22(15)+13(18b)	β(CCC)6b
22	510	–	533	519	1.97	0.00	85(16b)	τ(CCCC)16b
23	–	–	497	493	0.28	1.71	34(6a)+22(9a)+12(1)	β(CCC)6a
24	–	–	479	459	0.92	0.16	60(16a)+11[ω(OH)]+11(17b)+10(10a)	τ(CCCC)16a
25	–	–	367	359	0.69	1.04	31(15)+19(6a)+14[$\gamma(C_\alpha$—O)]+13(20a)+11(1)	$\beta(CCH_3)$15
26	–	–	345	324	1.41	0.39	66(18b)+12(15)+11[$\gamma(C_\alpha$—O)]	β(CF)18b
27	–	248	276	244	0.47	0.85	49(17b)+20(10b)+13(16a)	π(CF)17b
28	–	217	223	222	0.12	0.06	41(9a)+35[$\gamma(C_\alpha$—O)]+14(18b)	$\beta(CC_\alpha)$9a
29	–	–	202	204	0.88	0.82	85 π(C—CH_3)	$\pi(CCH_3)$10b
30	–	80	99	96	0.10	0.04	61(16a)+15(10a)+14[$\tau(CH_3)$]	$\pi(CC_\alpha)$10a
(ii) Vibrations of acid group								
31	–	3460	3774	3454	29.41	66.19	100[ν(OH)]	ν(OH)
32	1677	–	1781	1677	100.0	40.46	61[$\nu(C_\alpha$═O)]	$\nu(C_\alpha$═O)
33	–	–	1357	1359	11.61	0.74	35[δ(OH)]+17[$\nu(C_\alpha$═O)]+12[$\nu(C_\alpha$—O)]+10[$\delta(C_\alpha$═O)]	δ(OH)
34	–	–	1154	1148	35.39	2.00	23[$\nu(C_\alpha$—O)]+12[δ(OH)]+11(9b)	$\nu(C_\alpha$—O)
35	756	–	771	760	25.81	0.01	65(11)+24[$\omega(C_\alpha$═O)]	$\omega(C_\alpha$═O)
36	692	–	694	694	17.45	11.56	51[$\delta(C_\alpha$═O)]+15(1)	$\delta(C_\alpha$═O)
37	576	–	590	576	23.89	1.39	49[ω(OH)]+39[δ(OH)]	ω(OH)
38	–	–	403	385	0.47	1.18	27[$\gamma(C_\alpha$—O)]+23(6a)+19(15)+10(20a)	$\gamma(C_\alpha$—O)
39	–	–	52	49	0.16	0.03	36[$\tau(CC_\alpha)$]+32[$\tau(CH_3)$]+11[ω(OH)]	$\tau(CC_\alpha)$
(iii) Vibrations of methyl group								
40	2811	–	3257	2811	2.38	100.00	100[$\nu_s(CH_3)$]	$\nu_s(CH_3)$
41	2868	–	3146	2877	1.80	33.18	100[$\nu_{as}(CH_3)_{ip}$]	$\nu_{as}(CH_3)_{ip}$
42	–	2942	3107	2942	2.67	27.79	100[$\nu_{as}(CH_3)_{op}$]	$\nu_{as}(CH_3)_{op}$
43	1382	1386	1420	1382	1.62	5.23	80[$\delta_s(CH_3)$]	$\delta_s(CH_3)$
44	1444	1430	1471	1443	2.69	4.25	52[$\delta_{as}(CH_3)_{ip}$]+14(19a)+10[$\delta_s(CH_3)$]	$\delta_{as}(CH_3)_{ip}$
45	1463	–	1489	1463	2.64	3.81	92[$\delta_{as}(CH_3)_{op}$]	$\delta_{as}(CH_3)_{op}$
46	1037	–	1043	1037	32.31	0.20	41[$\gamma(CH_3)_{ip}$]+23[$\nu(C_\alpha$—O)]+10(1)	$\gamma(CH_3)_{ip}$
47	–	–	1057	1043	0.54	0.01	67[$\gamma(CH_3)_{op}$]+13(4)	$\gamma(CH_3)_{op}$
48	–	–	163	151	0.10	0.35	82[$\tau(CH_3)$]	$\tau(CH_3)$

–: Not observed.

[a] Relative infrared and Raman intensities are normalized to 100.

[b] Number before the parenthesis is % of PED. Number in the parenthesis is vibrational mode. PED less than 10 % is not shown.

[c] Mode in Wilson's notation [37]. C_α refers to Carbon atom of acid group and ν, stretching; β, in-plane bending; δ, deformation; γ, rocking; ω, wagging; π, out-of-plane bending; τ, torsion; s, symmetric; as, asymmetric; ip, in-plane; op, out of plane.

and one twisting vibration, $\tau(CH_3)$ in both groups in the three molecules. In addition to these nine vibrations, there are three more vibrations in CMA, viz $\nu(O'CH_3)$, $\delta(CO'C)$ and $\tau(O'CH_3)$.

The symmetric and asymmetric stretching vibrations of both groups generally occur in the range 2850–3000 cm^{-1}, whereas the out-of-plane stretching mode is expected around 2980 cm^{-1} [39]. The symmetric and asymmetric deformations of the methyl group represented by δ_sCH_3 and $\delta_{as}CH_3$ usually appear in the range 1375–1500 cm^{-1} in methyl- and methoxybenzenes, while the in-plane and out-of-plane rocking vibrations normally occur in the range 990–1040 cm^{-1} in methyl group and extended the range up to 1200 cm^{-1} in methoxy group [38], whereas the twisting modes occur around 50–150 cm^{-1} in both groups [38,39].

Thus, the weak absorptions near 2811, 2868 and 2942R cm^{-1} are identified as $\nu_s(CH_3)$, $\nu_{as}(CH_3)_{ip}$, and $\nu_{as}(CH_3)_{op}$ vibrations; while the strong absorptions near 1382, 1444 and 1463 cm^{-1} are assigned to $\delta_s(CH_3)$, $\delta_{as}(CH_3)_{ip}$ and $\delta_{as}(CH_3)_{op}$ modes, whereas frequencies obtained at 1037, 1043C* (C* indicates DFT computed value) and 151C cm^{-1} are attributed to $\gamma(CH_3)_{ip}$, $\gamma(CH_3)_{op}$ and $\tau(CH_3)$ vibrations, respectively in FMA. Similarly, the frequencies at 2892C, 2952R, 3000R, 1401, 1460, 1486C, 998, 1034 and 72C cm^{-1} are assigned to the corresponding modes of methyl group in BMA, respectively. In CMA, these vibrational modes are recognized at 2858R, 2951, 2985, 1449R, 1454C, 1461, 1121, 1172R and 115R cm^{-1}, while the other three vibrations $\nu(O'CH_3)$, $\delta(CO'C)$ and $\tau(O'CH_3)$ of methoxy group are found at 988, 332R and 126C cm^{-1}, respectively. It can be understood from the Tables 2–4 that the most of the vibrations associated with the methyl and methoxy

Table 3
Observed, calculated frequencies (in cm^{-1}) with DFT/6-311++G(d,p) and vibrational assignment of CMA.

S. no.	Obs. freq. (cm^{-1}) IR	Raman	Cal. freq. (cm^{-1}) Un-scaled	Scaled	Intensity[a] IR (I_i)	Raman (S_i)	Vibrational assignment[b]	Mode identification[c]
(i) Vibrations of aromatic unit								
1	–	3074	3210	3074	0.81	100.00	99(2)	ν(CH)2
2	–	3074	3202	3066	0.17	71.30	99(20b)	ν(CH)20b
3	3035	–	3185	3050	0.87	47.60	99(7a)	ν(CH)7a
4	1584	1591	1626	1589	9.94	31.88	60(8b)+19(18a)+12(6b)	ν(CC)8b
5	1561	1566	1601	1563	5.23	9.47	61(8a)+20(18a)+11(6b)	ν(CC)8a
6	–	1473	1481	1473	3.01	1.40	59(18b)+27(19b)	ν(CC)19b
7	1414	1402	1448	1411	20.49	0.35	36[$\delta_s(CH_3)$]+29(19a)+16(3)	ν(CC)19a
8	–	1277	1312	1271	4.13	4.64	69(14)+17(3)	ν(CC)14
9	–	1243	1273	1247	6.45	2.12	39(14)+16(13)+10(3)	β(CH)3
10	1236	–	1242	1226	15.42	22.48	26(14)+24(13)+17(3)	ν(CO′)13
11	–	1199	1211	1197	4.04	11.38	41(3)+25(14)+11(20a)	ν(CC_α)20a
12	1152	1152	1171	1148	10.11	5.72	29(14)+19(12)+15(9b)+14(7b)	β(CH)9b
13	1073	–	1095	1056	16.96	4.83	46(1)+23[ν(C_α—O)]+10(18a)	β(CH)18a
14	–	–	1003	983	0.18	0.28	64(5)+33(4)	π(CH)5
15	919	–	945	927	0.03	0.04	69(17a)+21(16a)	π(CH)17a
16	830	–	844	837	1.69	0.89	34(12)+20(20a)	β(CCC)12
17	799	801	829	813	3.82	4.35	36(4)+22(10a)+13(11)	π(CH)11
18	710	–	725	715	0.88	0.27	59(4)+10(17b)+11(10b)	τ(CCCC)4
19	605	–	602	604	1.27	2.99	23(4)+16(12)+11[β(O-CH3)]	ν(CC)1
20	584	–	591	589	1.32	2.52	45(16b)+10(15)+8(6b)	β(CCC)6b
21	549	550	554	557	1.59	2.36	82(16b)	τ(CCCC)16b
22	–	–	397	407	2.60	2.20	26(16b)+14(10b)+14(10a)+11(17b)	τ(CCCC)16a
23	–	394	391	398	0.20	1.28	17(15)+16(6a)+15(16a)+13[γ(C_α—O)]	β(CO′)15
24	–	372	396	376	2.85	5.65	29(12)+13(7b)+10(13)	ν(CCl)7b
25	–	–	337	347	1.03	2.43	18(16a)+16(6a)+12(10a)	β(CCC)6a
26	–	293	303	288	3.09	1.08	32(9a)+31(18b)	β(CCl)18b
27	–	206	205	208	0.17	0.77	82(17b)	π(CCl)17b
28	–	–	194	183	1.16	0.52	41(9a)+33(18b)	β(CC_α)9a
29	–	–	179	168	0.16	1.47	36(10b)+23(16a)+16(10a)	π(CC_α)10a
30	–	70	85	79	0.84	0.85	30(16a) + 18[ω(C_α═O)] +17 [ω (OH)]+ 13[τ(O′-CH_3)] + 7(10b)	π(CO′)10b
(ii) Vibrations of acid group								
31	–	3228	3559	3236	73.43	20.60	100[ν(OH)]	ν(OH)
32	1668	–	1809	1669	92.40	35.51	72[ν(C_α═O)]	ν(C_α═O)
33	–	–	1415	1324	100.0	3.03	50[δ(OH)]+15[ν(C_α═O)]	δ(OH)
34	–	1099	1114	1095	3.94	11.94	24[ν(C_α—O)]+18(12)+16(1)+10[γ(C_α—O]+10(18a)	ν(C_α—O)
35	750	753	798	758	10.35	0.77	69[ω(C_α═O)]+24[ω(OH)]	ω(C_α═O)
36	–	–	697	684	6.65	5.26	43[δ(C_α═O)]+17[γ(C_α—O)]	δ(C_α═O)
37	–	–	594	582	26.64	0.29	35[ω(OH)]+32(11)+10[ω(C_α═O)]+10(10a)	ω(OH)
38	–	–	417	414	0.60	3.82	22[γ(C_α—O)]+11(7b)	γ(C_α—O)
39	–	–	69	60	1.28	0.37	36[τ(CC_α)]+28[ω(OH)]+16[ω(C_α═O)]+13(16a)	τ(CC_α)
(iii) Vibrations of the methoxy group								
40	–	2858	3038	2875	8.74	79.39	100[$\nu_s(CH_3)$]	$\nu_s(CH_3)$
41	2951	2956	3121	2955	3.48	27.86	100[$\nu_{as}(CH_3)_{ip}$]	$\nu_{as}(CH_3)_{ip}$
42	2985	–	3154	2985	2.34	56.18	100[$\nu_{as}(CH_3)_{op}$]	$\nu_{as}(CH_3)_{op}$
43	–	1449	1489	1450	6.32	5.81	86[$\delta_s(CH_3)$]	$\delta_s(CH_3)$
44	–	–	1493	1454	7.93	1.70	60[$\delta_{as}(CH_3)_{ip}$]+15(19a)	$\delta_{as}(CH_3)_{ip}$
45	1461	–	1501	1460	1.78	4.70	88[$\delta_{as}(CH_3)_{op}$]+10[$\gamma(CH_3)_{op}$]	$\delta_{as}(CH_3)_{op}$
46	1121	1116	1164	1125	1.90	2.88	90[$\gamma(CH_3)_{ip}$]	$\gamma(CH_3)_{ip}$
47		1172	1199	1167	1.42	1.01	73[$\gamma(CH_3)_{op}$]	$\gamma(CH_3)_{op}$
48	988	992	998	988	20.68	5.78	73[ν(O′-CH_3)]	ν(O′CH_3)
49	–	332	350	336	1.15	3.26	34(16b)+28[δ(CO′C)]	δ(CO′C)
50	–	–	139	126	0.81	0.44	29[ω(OH)]+24[τ(O′-CH_3)]+10[ω(C_α═O)]	τ(O′CH_3)
51	–	115	129	115	0.09	0.06	41[τ(CH_3)]+20[ω(OH)]+15[ω(C_α═O)]+13[τ(O′-CH_3)]	τ(CH_3)

–: Not observed.

[a] Relative infrared and Raman intensities are normalized to 100.

[b] Number before the parenthesis is % of PED. Number in the parenthesis is vibrational mode. PED less than 10 % is not shown, exceptions being the modes at S. No. 21, 23, and 30.

[c] Mode in Wilson's notation [37], C_α refers to Carbon atom of acid group and prime (′) on the oxygen refers to methoxy group; ν, stretching; β, in-plane bending; δ, deformation; γ, rocking; ω, wagging; π, out-of-plane bending; τ, torsion; s, symmetric; as, asymmetric; ip, in-plane; op, out of plane.

group are pure as the mixing of PED from other vibrations is meagre or even no mixing. The assignments of the vibrational frequencies suggested here for methyl group of FMA and BMA; and methoxy group in CMA are in good agreement with those made in case of 4-methoxy-2-methyl benzoic acid [10]; monohalogenated anisoles [38]; and nitrotoluenes, dimethylanilines and trimethylbenzenes [39].

3.2.3. Acid group vibrations

There are nine vibrations associated with acid group in the three molecules under study and are represented as ν(O—H), ν(C_α═O), δ(OH), ν(C_α—O), ω(C_α═O), ω(OH), δ(C_α═O), γ(C_α—O) and τ(CC_α). The worthy feature of this acid group is that it involves in the intra-molecular interaction to form hydrogen bonding. Many of the modes of this group, except ν(O—H) and ν(C_α═O), have the vibrational characteristic nature that falls in the spectral range 1380–400 cm^{-1} in which several other fundamental vibrations like C—H in-plane deformations, C—H waggings and CCCC torsions also exist. The mixed modes having C—C stretching character, OH deformation and CH_3 deformations are observed in the range 1350–1500 cm^{-1}, whereas the region 1500–1800 cm^{-1} includes few other C—C stretching and C═O stretching vibrations

Table 4
Observed, calculated frequencies (in cm^{-1}) with DFT/6-311++G(d,p) and vibrational assignment of BMA.

S. no.	Obs. freq. (cm^{-1})		Cal. freq. (cm^{-1})		Intensity[a]		Vibrational assignment[b]	Mode identification[c]
	IR	Raman	Un-scaled	Scaled	IR (I_i)	Raman (S_i)		
(i) Vibrations of aromatic unit								
1	–	3066	3209	3076	0.87	100.00	99(2)	ν(CH)2
2	–	3066	3203	3071	0.09	40.19	99(20b)	ν(CH)20b
3	–	3066	3183	3051	0.93	45.87	99(7a)	ν(CH)7a
4	–	1632	1626	1628	2.40	21.04	62(8b)+21(18a)+10(6b)	ν(CC)8b
5	1586	1587	1593	1588	9.20	6.85	63(8a)+20(18a)	ν(CC)8a
6	–	–	1498	1495	6.53	1.02	47(18a)+28(19b)	ν(CC)19b
7	–	1448	1458	1448	2.69	0.42	46(19a)+27(3)	ν(CC)19a
8	1292	–	1305	1293	2.71	3.19	74(14)	ν(CC)14
9	1253	–	1247	1249	1.07	4.44	43(14)+31(3)	β(CH)3
10	–	1210	1220	1213	8.55	6.37	35(3)+32[δ(OH)]+21(14)+6(20a)	$\nu(CC_\alpha)$20a
11	–	1199	1201	1199	0.79	8.73	34(14)+26(13)+26(9b)	$\nu(CCH_3)$13
12	–	1164	1154	1162	19.54	1.96	20(1)+20[δ(OH)]+17(9b)+10(6b)	β(CH)9b
13	–	1102	1106	1098	4.44	17.51	32(12)+28(1)+10(18a)+10(13)	β(CH)18a
14	–	988	995	991	0.36	0.08	71(5)+24(4)	π(CH)5
15	–	936	942	939	0.07	0.10	82(17a)+15(16a)	π(CH)17a
16	833	–	827	831	1.05	0.90	46(12)+10(13)+10(20a)	β(CCC)12
17	808	–	822	810	3.34	0.18	48(11)+28(4)+14(10a)	π(CH)11
18	–	784	778	775	3.69	5.61	33(6a)+18(13)+17(1)+13(7b)	ν(CC)1
19	749		770	757	16.26	0.37	36(11)+30(4)+14(10a)	τ(CCCC)4
20	–	547	576	563	2.02	7.06	36(6b)+19(13)+14[$\delta(C_\alpha{=}O)$]+13(1)	β(CCC)6b
21	–	–	513	481	0.84	0.11	47(16b)+13[$\omega(C_\alpha{=}O)$]+11(10b)	τ(CCCC)16b
22	–	–	466	439	0.50	0.86	92(16a)	τ(CCCC)16a
23	–	380	381	380	2.03	1.07	42(6a)+17[$\delta(C_\alpha{=}O)$]+13(20a)	β(CCC)6a
24	–	–	376	360	0.58	0.35	57(4a)+18[$\gamma(C_\alpha{-}O)$]+11(15)	$\beta(CCH_3)$15
25	–	289	300	287	0.32	1.33	40(18b)+26(7b)+14(6a)	ν(CBr)7b
26	–	260	276	265	0.16	3.13	31(7b)+22(18b)+15(9a)+10[$\gamma(C_\alpha{-}O)$]	β(CBr)18b
27	–	196	238	194	1.24	0.67	66(16a)+16(10b)	$\pi(CCH_3)$10b
28	–	–	176	159	0.17	0.57	40(9a)+25(18b)+10(16a)	$\beta(CC_\alpha)$9a
29	–	–	169	132	0.23	1.00	55(16a)+19(17b)+11[$\tau(CC_\alpha)$]+7(10a)	$\pi(CC_\alpha)$10a
30	–	–	143	122	0.25	0.30	49(17b)+19[$\tau(CC_\alpha)$]+13(16a)	π(CBr)17b
(ii) Vibrations of acid group								
31	–	3370	3756	3371	23.28	93.55	100[ν(OH)]	ν(OH)
32	1677	–	1779	1677	100.00	56.59	62[$\nu(C_\alpha{=}O)$]+17(20a)	$\nu(C_\alpha{=}O)$
33	1378	1378	1360	1376	36.81	3.46	22(20a)+18[δ(OH)]+17(3)+10[$\nu(C_\alpha{=}O)$]+10(6a)	δ(OH)
34	1077	1084	1090	1080	39.08	3.47	41[$\nu(C_\alpha{-}O)$]+30(1)	$\nu(C_\alpha{-}O)$
35	687	683	706	702	0.57	0.36	62(4)+15[$\omega(C_\alpha{=}O)$]	$\omega(C_\alpha{=}O)$
36	–	–	662	653	16.52	6.09	44[$\delta(C_\alpha{=}O)$]+27(6b)	$\delta(C_\alpha{=}O)$
37	589	588	611	568	19.50	1.43	50[$\omega(C_\alpha{=}O)$]+49[ω(OH)]	ω(OH)
38	–	535	556	537	0.23	0.46	28(15)+17[$\gamma(C_\alpha{-}O)$]+11(9a)	$\gamma(C_\alpha{-}O)$
39	–	71	95	71	0.12	0.60	23[$\tau(CC_\alpha)$]+16[$\tau(CH_3)$]+15(16a)+15(17b)	$\tau(CC_\alpha)$
(iii) Vibrations of methyl group								
40	–	–	3046	2892	1.50	76.34	100[$\nu_s(CH_3)$]	$\nu_s(CH_3)$
41	–	2952	3116	2958	2.68	73.97	100[$\nu_{as}(CH_3)_{ip}$]	$\nu_{as}(CH_3)_{ip}$
42	–	3000	3153	2993	1.26	22.04	100[$\nu_{as}(CH_3)_{op}$]	$\nu_{as}(CH_3)_{op}$
43	1401	–	1422	1401	0.92	6.90	84[$\delta_s(CH_3)$]	$\delta_s(CH_3)$
45	–	–	1467	1460	3.31	2.64	63[$\delta_{as}(CH_3)_{op}$]+10[$\delta_{as}(CH_3)_{ip}$]	$\delta_{as}(CH_3)_{ip}$
44	–	–	1489	1486	4.71	3.64	76[$\delta_{as}(CH_3)_{ip}$]	$\delta_{as}(CH_3)_{op}$
46	998	–	1022	998	7.28	1.00	56[$\gamma(CH_3)_{ip}$]+15(1)	$\gamma(CH_3)_{ip}$
47	1034	–	1054	1035	2.37	0.21	65[$\gamma(CH_3)_{op}$]	$\gamma(CH_3)_{op}$
48	–	–	87	72	0.13	0.63	62[$\tau(CH_3)$]+14[$\tau(CC_\alpha)$]	$\tau(CH_3)$

–: Not observed.

[a] Relative infrared and Raman intensities are normalized to 100.

[b] Number before the parenthesis is % of PED. Number in the parenthesis is vibrational mode. PED less than 10 % is not shown, exceptions being the modes at S. No. 10, and 29.

[c] Mode in Wilson's notation [37]. C_α refers to Carbon atom of acid group and ν, stretching; β, in-plane bending; δ, deformation; γ, rocking; ω, wagging; π, out-of-plane bending; τ, torsion; s, symmetric; as, asymmetric; ip, in-plane; op, out of plane.

to occur [40]. CH_3 stretching vibrations of methyl or methoxy group; C—H stretching mode of aromatic nucleus; and O—H stretching vibration of COOH group occur in the spectral region over 2840–3500 cm^{-1}.

The vibrations associated with O—H bond are very sensitive due to the intra-molecular interaction that instigates the formation of hydrogen bonding. The O—H stretching band is normally demonstrated by a very broad band occurring in the region about 3400–3600 cm^{-1}. But, a group of atoms of substituent facing a change in its environment due to intra-molecular interaction exhibits a frequency shift towards lower side in IR absorption so as to fall within 3200–3500 cm^{-1} region. Thus, the frequency bands observed at 3460, 3228 and 3370 cm^{-1} are assigned to ν(O—H) stretching vibration in FMA, CMA and BMA, respectively. It is a pure mode with 100 % PED from O—H stretching character which can be evidenced from Tables 2–4.

The carbonyl stretch $\nu(C{=}O)$ of carboxylic acid group appears as an intense band in the range 1660–1760 cm^{-1}. The position of this band depends on the hydrogen bonding due to intra-molecular interaction of carboxylic acid group [41]. The strong IR absorptions near 1677, 1668 and 1677 cm^{-1} are assigned to the mode $\nu(C_\alpha{=}O)$ in FMA, CMA and BMA, respectively.

The vibrations $\nu(C_\alpha{-}O)$ and δ(OH) of acid group are influenced by the bonding of atoms whether they are dimeric, monomeric or other hydrogen bonding. Normally, they occur in the spectral region of 1050–1400 cm^{-1}. It is established fact that δ(OH) visible at a greater

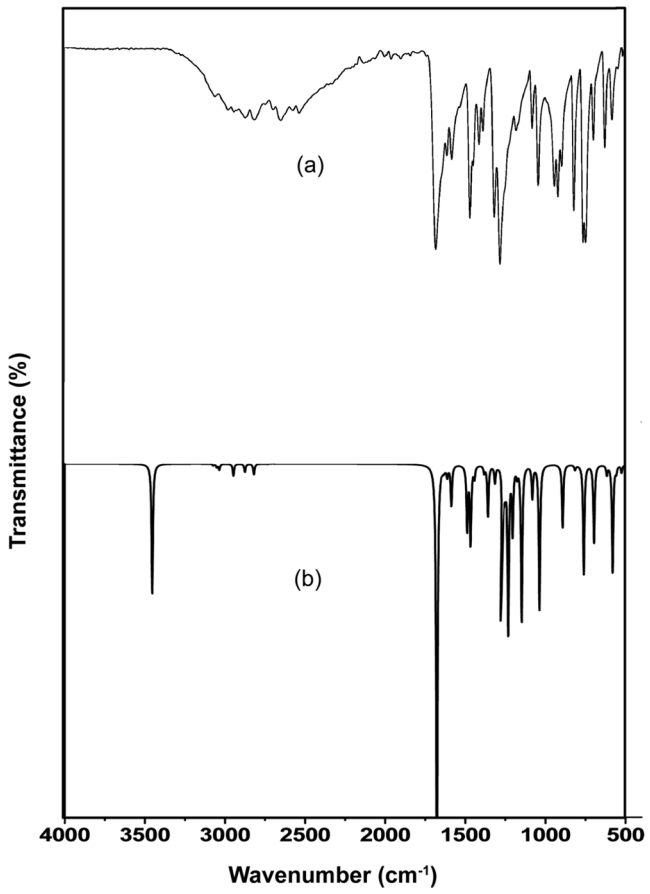

Fig. 2. FT-IR Spectrum of FMA (a) Experimental and (b) Simulated with DFT/B3LYP/6-311++G(d,p) formalism.

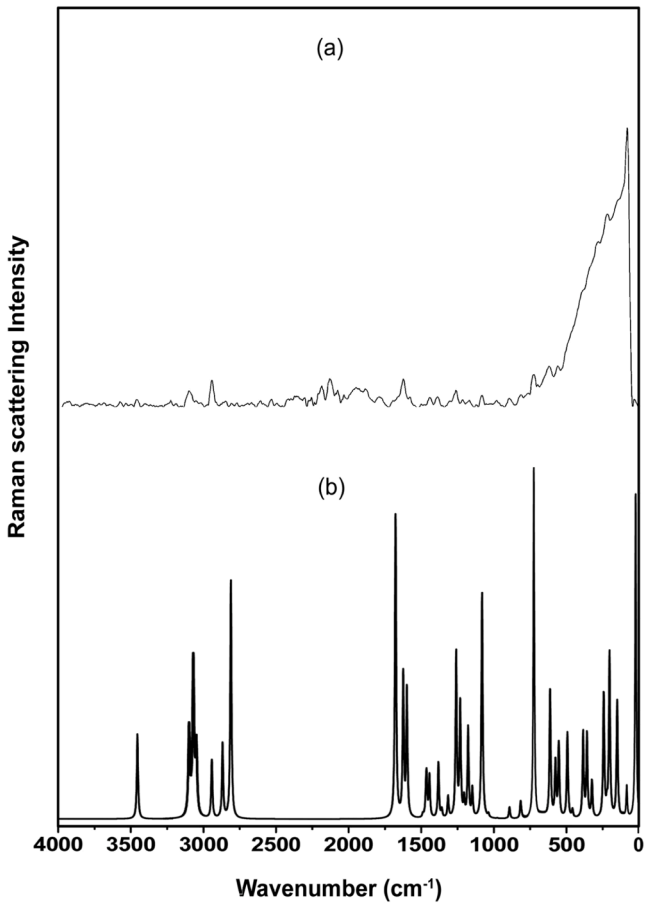

Fig. 3. FT-Raman Spectrum of FMA (a) Experimental and (b) Simulated with DFT/B3LYP/6-311++G(d,p) formalism.

frequency than that of $\nu(C_\alpha—O)$ and overlap with other bands. Thus, the frequencies near 1359C and 1148; 1324C and 1099R; and 1378 and 1077 cm^{-1} are attributed to δ(OH) and $\nu(C_\alpha—O)$ in FMA, CMA and BMA. These vibrations are associated with some other modes which occur in the same spectral region as can be seen from Tables 2–4. The deformations, $\delta(C_\alpha═O)$ and $\gamma(C_\alpha—O)$, associated with this acid group are identified at 692 and 385C cm^{-1}; 684C and 414C cm^{-1}; and 662C and 535R cm^{-1} in FMA, CMA and BMA, respectively based on the PED obtained in the computations. Similarly, the pair of bands near 756 and 576 cm^{-1}; 750 and 582C cm^{-1}; and 687 and 589 cm^{-1} are assigned to $\omega(C_\alpha═O)$ and ω(OH) out-of-plane bending vibrations in FMA, CMA and BMA, respectively. Further, the frequency calculated at 49C and 60C cm^{-1} in FMA and CMA, respectively; and Raman shift observed at 71R cm^{-1} in BMA is attributed to torsion $\tau(CC_\alpha)$. All the assignments of fundamental vibrations of acid group in the three molecules are in good accordance with literature values [10,41] and with our earlier assignments for bipyridine di-carboxylic acids [42]; and picolinic and isonicotinic acids [43].

3.3. NMR spectral analysis

NMR spectroscopy facilitates greatly to determine the structure of an organic molecule by enlightening its hydrogen and carbon skeleton. Hence, the ^1H and ^{13}C NMR chemical shifts were measured for the molecules FMA, CMA and BMA in a solution of DMSO-d_6. They were determined theoretically also as discussed in the preceding Section 2.2 dealt with computational aspects so as to make an explicit analysis of ^1H and ^{13}C NMR spectra. The experimental ^1H and ^{13}C NMR spectra of these molecules are depicted in Figs. SF1 and SF2 as supplementary information and are compared with the corresponding simulated values in Table 5.

The ^1H and ^{13}C NMR spectra help to study the conformers and molecular properties like solubility, phase changes, and dispersion [44]. The experimental ^1H chemical shifts of FMA are observed in the range near 2.449–13.139 ppm with associated theoretical proton chemical shift values are in the region over 2.516–12.321 ppm, while in CMA, they are observed in the span of 3.822–13.241 ppm with corresponding theoretical values in the range 4.140–12.911 ppm, whereas those of BMA are observed in the region 2.493–13.235 ppm which are accorded well with the theoretical values occurred in the range 2.551–12.741 ppm. It can be observed from the Table 5 that the chemical shifts of three hydrogen atoms; H16, H17 and H18 of methyl group in FMA and BMA; and H17, H18 and H19 of methoxy group in CMA are observed in the low range over 2.449 - 3.822 ppm due to the low electronic charge density around them. Further, the chemical shift value for H15 in acid group in the three molecules is deviated by large value due to the neighbouring electronegative oxygen atom.

Generally, ^{13}C NMR chemical shifts of organic molecule will be greater than 100 ppm [45,46]. Experimental ^{13}C chemical shifts are observed in the range over 11.955–168.356 ppm; 62.073–166.883 ppm; and 20.710–168.952 ppm in accordance with theoretical values in the region 14.030–171.867 ppm; 62.707–170.226 ppm; and 22.755–174.885 ppm, respectively in FMA, CMA and BMA. It is evident from Table 5 that the chemical shift value of carbon, C7 of acid group is high due to the more electronegative effect of neighbour oxygen atoms O13 and O14. Similarly, the chemical shift value of carbon atom, C8 of methyl group and C16 of methoxy group is lowered due to the low electronic charge density around them.

The experimental and theoretical chemical shift values are in good agreement with each other. However, the computed chemical shifts are

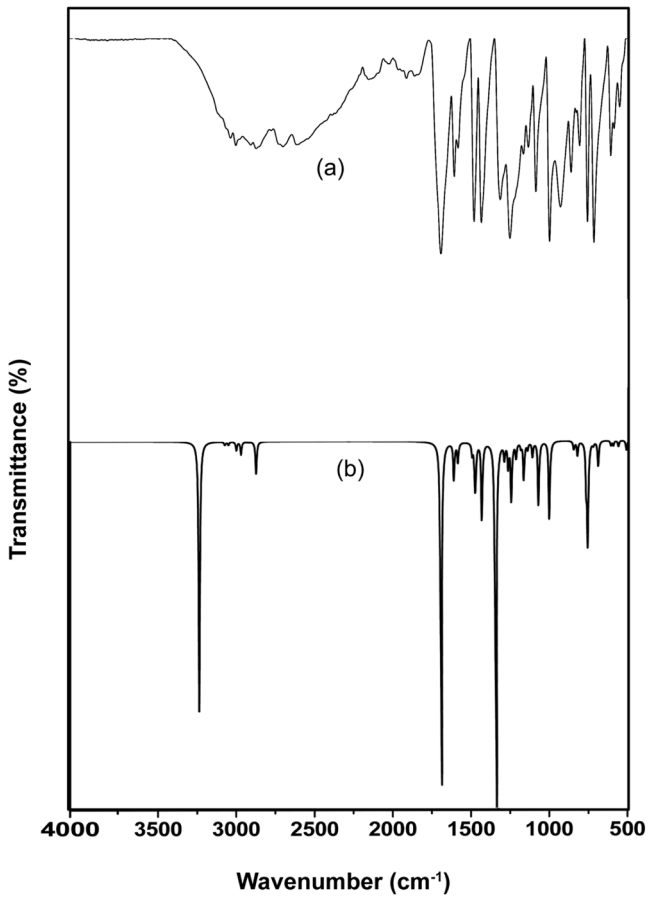

Fig. 4. FT-IR Spectrum of CMA (a) Experimental and (b) Simulated with DFT/B3LYP/6-311++G(d,p) formalism.

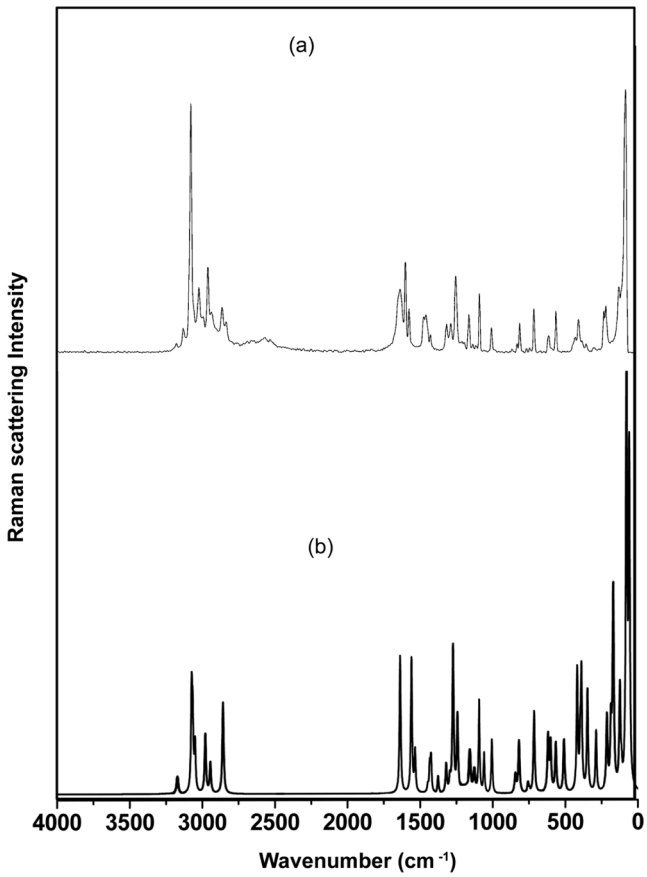

Fig. 5. FT-Raman Spectrum of CMA (a) Experimental and (b) Simulated with DFT/B3LYP/6-311++G(d,p) formalism.

somewhat greater from the observed results due to the fact that the DFT computations were performed in gas phase, whereas the experimental values were obtained in the solid state.

3.4. Analysis of UV–visible spectra and frontier molecular orbitals (FMOs)

Any given organic compound can be analysed quantitatively with the help of UV–visible spectra. But, this technique will be ineffective if the organic compound is contaminated during the production process. This problem can be overcome by either isolating all the impurities in the compound or re-synthesize the impurities separately. But, this process is time consuming and cost effective, which instigated to explore the theoretical methods focusing at the simulation of UV–visible spectra of the organic compound for its quantitative analysis. The variational quantum eigensolver approach, suggested by Parish et al. [47], is useful to compute the electronic transitions, by which the various theoretical formalisms have been developed to simulate UV–vis spectra and to evaluate other corresponding parameters. The Time-dependent density functional theory (TD-DFT) is one of them which were used by earlier researchers for getting better results rationally for determining the UV–visible spectral parameters [48–50]. Hence, the same method was used in these investigations.

The observed UV–vis spectra exhibit a broad absorption in the three molecules due to line broadening effects like Doppler effect, thermal excitement and natural line width, whereas its simulated counterpart is in the form of a line. Hence, the simulated spectra need the broadening to appear as a Gaussian shape [51,52]. Thus, the UV–visible absorption spectra was simulated by following the integrated method proposed by Bremond et al. [53] to achieve the Gaussian shape having a pre-assigned full width at half maximum (FWHM) by independent optimization for each Gaussian function from the line spectra obtained by TD-DFT. This method has yielded results with good agreement between experimental and simulated [53].

The simulated UV–visible spectra of the three molecules were obtained by following the three steps given below [54,55]:

(a) Fully optimized ground state molecular geometry
(b) Ensuring the appropriate number of vibrational frequencies without absence of negative frequencies or imaginary frequencies to establish the molecular structure with global minimum energy.
(c) Simulation of UV–vis spectra by evaluating vertical transitions to valence excited states theoretically.

The first two processes were implemented as a part of our DFT computations, whereas the last step is executed employing TD-DFT.

UV–visible spectra are simulated using at TD-DFT/B3LYP/6-311++G(d,p) level of theory for the three molecules in DMSO-d_6 solvent. The solvent effects were taken care by including a variant of polarizable continuum model (PCM), known as integrated equation formalism PCM (IEF-PCM) [56] so as to fit into Gaussian 09 W program. The experimental and simulated spectra are shown in Fig. 8 for the three molecules under investigation. The experimental and calculated electronic transition maxima (λ_{max}) are portrayed in Table 6 along with the corresponding excitation energies, wavelengths and oscillator strengths.

From Fig. 8 and Table 6, it can be seen that the electronic absorption maxima were observed at 232 and 276 nm; 224 and 281 nm; and 236 and 278 nm in FMA, CMA and BMA, respectively and coincided with the simulated counterparts at 237.08 and 272.90 nm; 236.54 and 271.91 nm; and 237.16 and 277.16 nm.

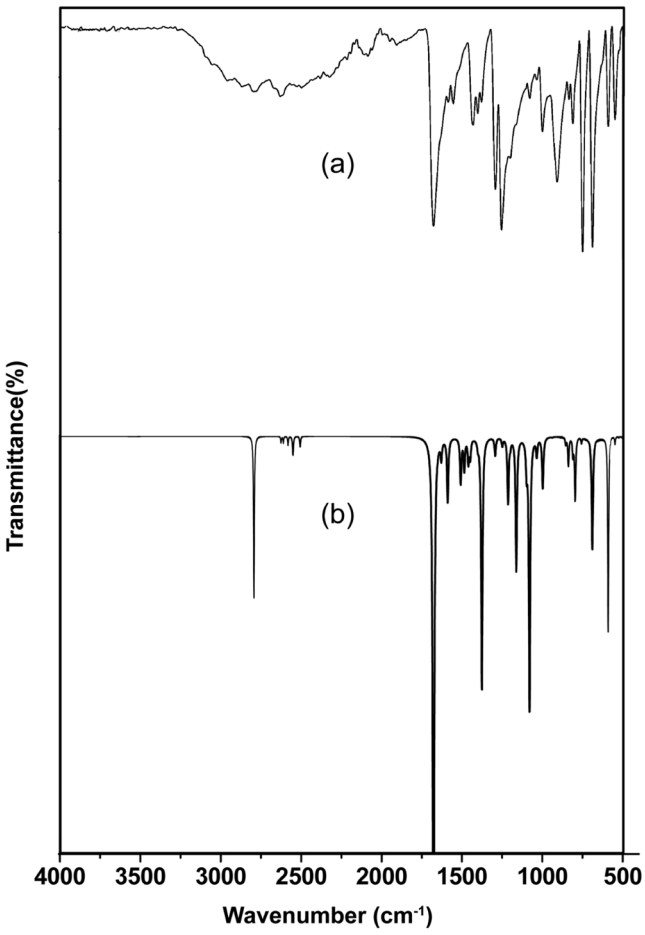

Fig. 6. FT-IR Spectrum of BMA (a) Experimental and (b) Simulated with DFT/B3LYP/6-311++G(d,p) formalism.

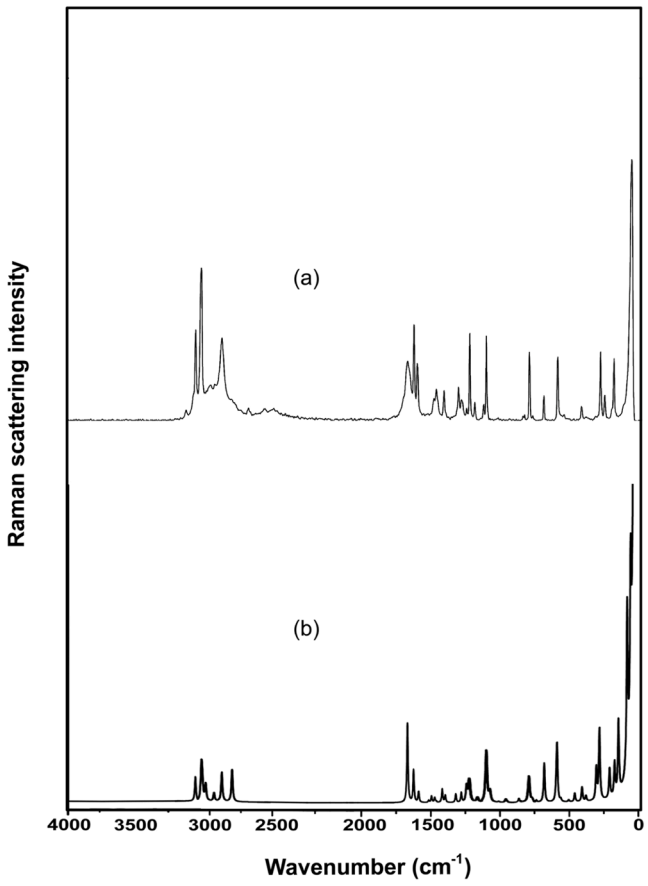

Fig. 7. FT-Raman Spectrum of BMA (a) Experimental and (b) Simulated with DFT/B3LYP/6-311++G(d,p) formalism.

It is established that the highest occupied molecular orbital (HOMO) and the lowest unoccupied molecular (LUMO) are considered together as frontier molecular orbitals (FMOs). They are depicted in Fig. 9 for the three molecules. They facilitate to know the type of electronic transitions involved to yield the absorption maxima in UV–visible spectra, which is analyzed in the previous paragraphs. FMOs demonstrate the ability of a molecule to absorb the electromagnetic radiation which causes the electronic transitions. HOMO behaves as the electron donor, whereas LUMO extends the role of an electron acceptor [57,58]. TD-DFT computations, as discussed in the preceding paragraphs, reveal that the absorption maxima obtained at 276, 281 and 278 nm are due to n → π* transition corresponding to the major contribution to the extent of 91 %, 87 % and 89 % from H → L in FMA, CMA and BMA, respectively. Similarly, the bands observed near 232, 224 and 236 nm are due to π → π* transition corresponding to H-1 → L in the three molecules. The absorption at 232 nm in FMA is due to major contribution only from H-1 → L (92 %) transition, whereas the band at 224 nm in CMA is resulted due to multiple contributions from H-2 → L (11 %) and H → L + 1 (11 %) in addition to H-1 → L (73 %), while the absorption maximum at 236 nm in BMA is resulted due to the contributions from H-1 → L (34 %), H-2 → L (29 %) and H-3 → L (22 %).

Table 5
Experimental and calculated ^{1}H and ^{13}C NMR chemical shifts (δ) of FMA, CMA and BMA in ppm.

Atom	FMA		CMA		BMA	
	Exp.	Cal.	Exp.	Cal.	Exp.	Cal.
H10	7.312	7.519	7.654	7.851	7.708	7.930
H11	7.371	7.528	7.222	7.490	7.223	7.451
H12	7.627	8.368	7.680	8.227	7.780	8.092
H15	13.139	12.321	13.241	12.911	13.235	12.740
H16	2.503	2.765	–	–	2.539	2.846
H17	2.496	2.517	3.822	3.587	2.501	2.654
H18	2.449	2.516	3.822	4.391	2.493	2.551
H19	–	–	3.822	4.140	–	–
C1	126.355	132.348	128.603	130.148	127.882	137.100
C2	133.490	138.908	155.016	162.588	135.627	148.523
C3	162.194	169.711	133.896	142.323	137.424	149.903
C4	118.646	125.783	130.055	141.897	134.476	143.100
C5	126.041	130.880	128.719	130.613	126.655	130.832
C6	127.421	134.528	125.476	137.358	129.391	137.159
C7	168.356	171.867	166.883	170.226	168.952	174.885
C8	11.955	14.030	–	–	20.710	22.755
C16	–	–	62.073	62.707	–	–

–: Not relevant.

3.5. Global reactivity descriptors

The global reactivity descriptors of the conjugated molecular system can be evaluated from the analysis of frontier molecular orbitals [59]. The associated parameters, like ionization energy (I), electron affinity (A), chemical hardness (η), chemical softness (s), chemical potential (μ) and electrophilicity power (ω) give insights into the polarizability, reactivity and kinetic stability of a molecule [60]. They are computed by employing DFT/B3LYP/6-311++G(d,p) level of theory and are depicted in Table 7 for FMA, CMA and BMA. The energy values of HOMO, LUMO and band gap between HOMO and LUMO are computed at −9.5278 eV, −5.6869 eV and 3.8409 eV for FMA; −8.3574 eV, −5.4678 eV and 2.8896 eV for CMA; and −9.5975 eV, −5.6420 eV and 3.9555 eV for

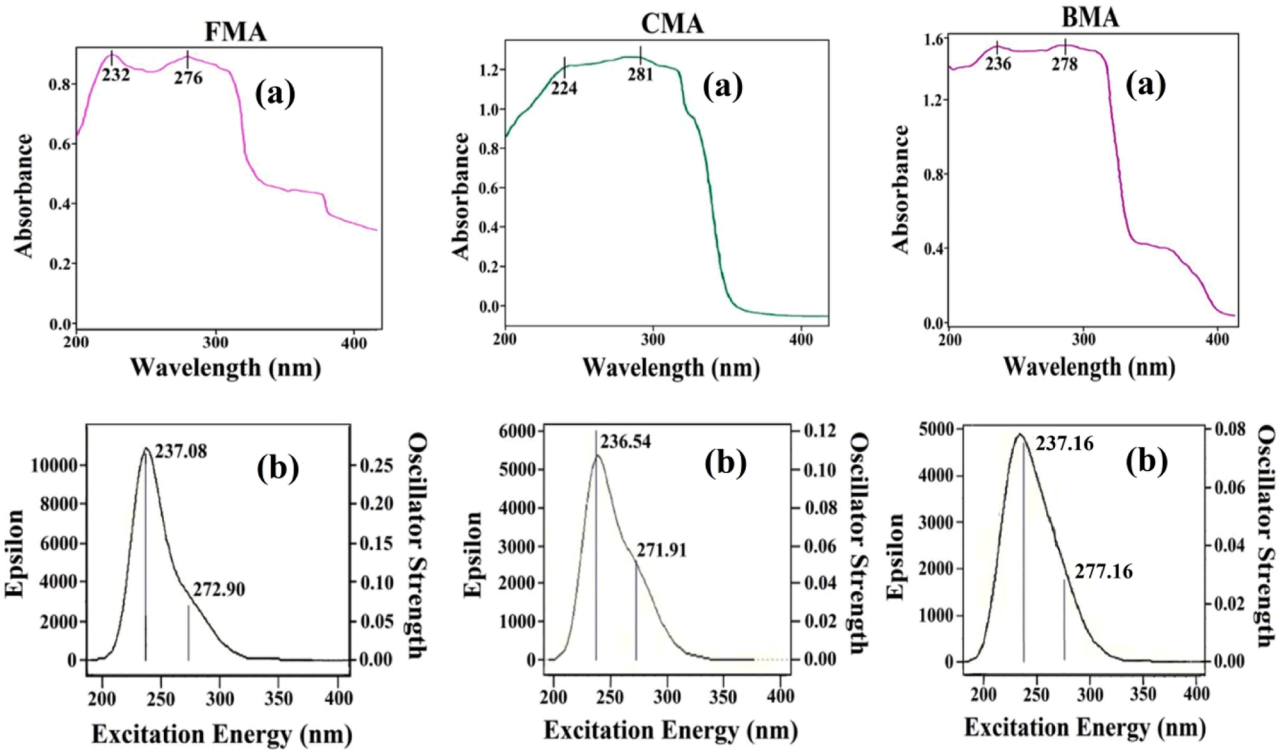

Fig. 8. UV–vis Spectrum of FMA, CMA and BMA (a) Experimental and (b) Simulated with TD-DFT/B3LYP/6-311++G(d,p)formalism.

Table 6
Experimental and theoretical (DFT/B3LYP/6-311++G(d,p) formalism) electronic absorption spectral values for FMA, CMA and BMA.

Compound	Absorption maximum, λ_{max} (nm)		Excitation energy (eV)	Oscillator Strengths (f)	Major contribution (>10 %)	Transition
	Expt.	Cal.				
FMA	276	272.90	4.5431	0.0693	H → L (91 %)	n → π*
	232	237.08	5.2296	0.2630	H-1 → L (92 %)	π → π*
CMA	281	271.91	4.560	0.0519	H → L (87 %)	n → π*
	224	236.54	5.242	0.1199	H-1 → L (73 %),H-2 → L (11 %), H → L + 1 (11 %)	π → π*
BMA	278	277.16	4.4735	0.0480	H → L (89 %)	n → π*
	236	237.16	5.2278	0.0523	H-1 → L (34 %),H-2 → L (29 %), H-3 → L (22 %)	π → π*

H: HOMO; L: LUMO.

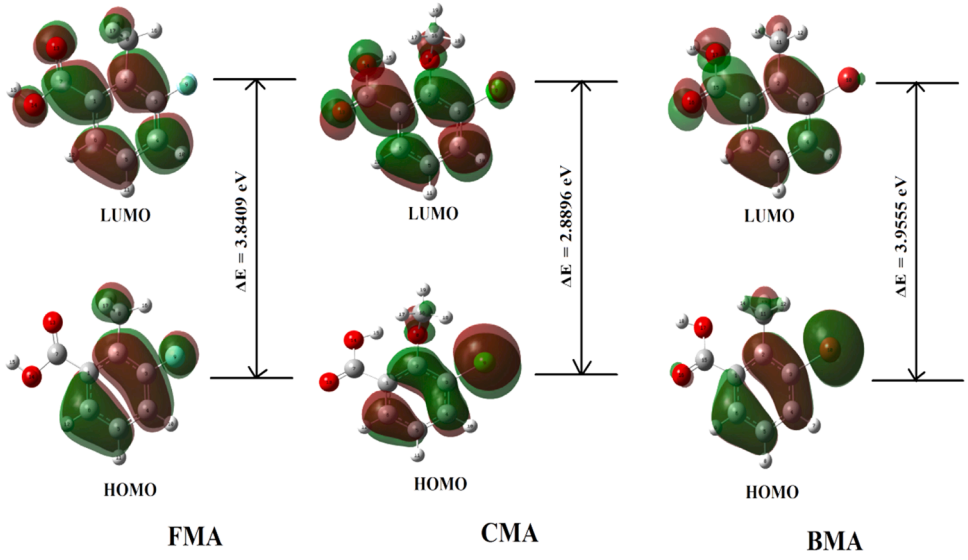

Fig. 9. Frontier molecular orbitals of FMA, CMA and BMA.

Table 7
Frontier molecular orbital parameters of FMA, CMA and BMA.

Frontier molecular orbital parameter	Value (in eV)		
	FMA	CMA	BMA
HOMO energy	−9.5278	−8.3574	−9.5975
LUMO energy	−5.6869	−5.4678	−5.6420
Frontier molecular orbital energy gap	3.8409	2.8896	3.9555
Ionization energy (I)	9.5278	8.3574	9.5975
Electron affinity (A)	5.6869	5.4678	5.6420
Global hardness (η)	1.9204	1.4448	1.9777
Global softness (S)	0.2604	0.3461	0.2528
Chemical potential (μ)	−7.6073	−6.9126	−7.6197
Electronegativity (χ)	7.6073	6.9126	7.6197
Global electrophilicity power (ω)	15.0674	16.5365	14.6786

BMA, respectively. The quantity of the energy gap is a characteristic feature of a conjugated system which reveals the polarizability and chemical reactivity of a molecule [61]. A molecule with small energy gap demonstrates the easy excitation from lower energy HOMO to higher energy LUMO that indicates the high polarizability and high chemical reactivity [62]. The negative value of the chemical potential (μ) of the three molecules demonstrates their high kinetic stability.

The value of chemical hardness (η) reveals the resistance shown by a given molecular system against the electronic structural changes, which is also a measure of chemical reactivity of that molecule [63]. From Table 7, it can be seen that the value of η is comparatively high for FMA and BMA over CMA. So, FMA and BMA offer high opposition for the changes in their electronic structure. Similarly, the larger value of electrophilicity power (ω) signifies the stabilization in energy when the molecule acquires an additional electronic charge from the neighbour atoms. The value of ionization potential tracks the order BMA > FMA > CMA, while the electron affinity value demonstrates the order FMA > BMA > CMA (Please refer Table 7). Further, the electronegativity (χ) determines the ability of an atom to attract electrons from the surrounding environment. The electronegativity values are computed at 7.607, 6.913 and 7.619, eV for FMA, CMA and BMA, respectively, which shows the good ability of attracting electrons from the adjacent atoms. Thus, it can be summarized from the computed reactivity descriptor values that the three molecules are chemically reactive, susceptive to polarize and highly stable.

3.6. Molecular electrostatic potential (MEP)

Molecular electrostatic potential (MEP) is a resourceful indicator to estimate the electrophilic and nucleophilic reactive regions of the molecule to know the biological identity [64] and hydrogen bond interaction [65], respectively. MEP surface of the molecules FMA, CMA and BMA were obtained from their optimized geometries. The 3D MEP diagram of these molecules is portrayed in Fig. 10. The electrostatic surface potential ranges from −8.731e−2 to 8.731e−2 a.u for FMA; −9.730e−2 to 9.730e−2 a.u for CMA and −9.363e−2 to 9.363e−2 a.u for BMA. The colour scheme for MEP surfaces changes as electron rich - neutral - electron deficit and is represented in the order as red < orange < yellow < green < blue. The red colour indicates the most negative site that represents the electrophilic reactivity, while blue colour signifies the most positive site indicating the nucleophilic reactivity, whereas the green colour shows the zero potential of the molecule. MEP maps exhibit that the region around the oxygen atom (O13) is more negative shown in red colour region and the remaining regions of the title molecules are blue colour indicating positive charge. The most positive potential is found around the hydrogen atom of acid group moiety in FMA and BMA; and around the fluorine atom and methyl group in CMA.

3.7. Non-linear optical (NLO) study

The interaction of an electromagnetic wave with NLO material causes to undergo changes in its optical properties like amplitude, frequency, or phase, thereby creates new electromagnetic field [66,67]. If these changes are predominant, then those materials offer their usage in NLO applications, like frequency modulation, optical logic, optical coupling and switching, and optical memory in telecommunications area [67,68]. Further, the optical property and the geometry of the molecule play a significant role in the field of opto-electronics for data storage, cutting edge communication technology and optical signal processing [69,70]. The three important parameters such as polarizability (α), first-order hyperpolarizability (β_t) and electric dipole moment (μ) are responsive in an applied electric field through finite-field methods, which provide information on the NLO behaviour of a given molecule. The polarizability of an atom or molecule is a quantity that signifies the easiness with which the nucleus and electrons can distort their stable state.

In the recent past, the density functional theory (DFT) method has become an important tool to study the organic and inorganic NLO materials in terms of these optical parameters. Thus, the polarizability (α), first order hyperpolarizability (β_t) and electric dipole moment (μ) components were evaluated using DFT/B3LYP method with 6-311++G (d,p) basis set employing finite field approach by integrating Gaussian 09 W program as discussed in the computational details section to study the NLO activity of the molecules under investigation. The mean polarizability (α_t), the anisotropy of polarizability (Δα), first order hyperpolarizability (β_t) and total static dipole moment (μ_t) values were calculated by using the equations given below, which are discussed in detail in our earlier paper [43] and are summarized in Table 8

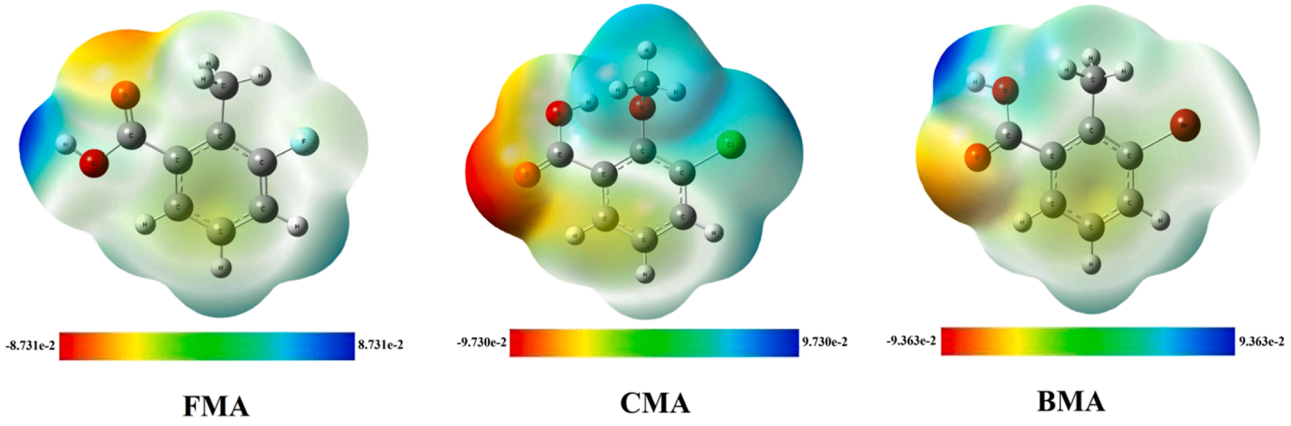

Fig. 10. Total electron density mapped with molecular electrostatic potential (MEP) surface of FMA, CMA and BMA.

Table 8
Values of dipole moment, μ_t (in Debye); polarizability, α_t in 1.4818×10^{-25} cm^3; and first order hyperpolarizability, β_t (in 10^{-30} cm^5/e.s.u) of FMA, CMA and BMA.

Frontier molecular orbital parameter	Value with B3LYP/6-311++G(d,p)		
	FMA	CMA	BMA
μ_x	−0.0915	−1.6979	0.0994
μ_y	0.8474	0.0836	- 0.0966
μ_z	0.0002	0.4877	0.2318
μ_t	**0.85**	**1.77**	**0.27**
α_{xx}	123.8482	146.6639	160.5128
α_{xy}	6.8854	4.7752	−2.3679
α_{yy}	117.5955	132.3168	130.8948
α_{xz}	−0.0006	2.2625	2.1409
α_{yz}	0.0020	3.6209	−0.4514
α_{zz}	56.7293	69.1153	70.5761
α_t	**99.3910**	**116.0320**	**120.6612**
$\Delta\alpha$	**64.2212**	**71.4635**	**79.3857**
β_{xxx}	−321.6125	−184.5944	−185.9043
β_{xxy}	−25.7659	−88.5255	−86.1322
β_{xyy}	−21.5983	12.4550	−78.4258
β_{yyy}	145.6234	89.7148	65.0183
β_{xxz}	0.0012	−296.2580	17.2809
β_{xyz}	0.0127	−71.2609357	−7.9627
β_{yyz}	−0.0184	10.8910	7.8963
β_{xzz}	1.2385	−328.3132	43.7343
β_{yzz}	54.3527	−66.5227	18.0980
β_{zzz}	−0.0084	−293.1586	16.8383
β_t	**3.316**	**6.634**	**1.941**

Mean polarizability, $\langle \alpha_t \rangle = 1/3\left[\alpha_{xx} + \alpha_{yy} + \alpha_{zz}\right]$,

First order hyperpolarizability, $\beta_t = \left[(\beta xxx + \beta xyy + \beta xzz)^2 + (\beta yyy + \beta yxz + \beta yzz)^2 + (\beta zzz + \beta xzz + \beta xyy)^2\right]^{1/2}$

and

Total dipole moment, $(\mu_t) = \left(\mu_x + \mu_y + \mu_z\right)^{1/2}$

In the present investigation, the dipole moment (μ_t) and hyperpolarizability (β_t) values are observed at 0.85 D and 3.316×10^{-30} cm^5/esu; 1.77 D and 6.634×10^{-30} cm^5/esu; and 0.27 D and 1.941×10^{-30} cm^5/esu in FMA, CMA, and BMA molecules, respectively. The prototypical molecule, Urea is widely accepted to consider as a standard NLO material since it is formed by the amalgamation of non-centrosymmetric crystal packing and intra-molecular charge transfer (ICT) ability. It is also considered as one of the standards among second harmonic generation (SHG) NLO materials. It exhibits the electro-optic effect which modifies the refractive index and second harmonic generation under the influence of external field due to scattering of light by the material at double the frequency of incident light. Further, Urea cannot demonstrate non-linearity over the visible absorbing molecules. Its second order non-linearity is significantly greater than that of other organic molecules like fluorobenzene, nitrobenzene, aniline, *p*-nitroaniline and merocyanine with comparable UV transparency [71]. Hence, the Urea is often considered as reference to investigate the NLO behaviour of a given molecule.

The total dipole moment (μ_t) and first order hyperpolarizability (β_t) values of the reference molecule, Urea are 1.3732 Debye and 0.3728×10^{-30} cm^5/esu. On comparing the value of β_t for the three molecules from Table 8 with these threshold values, it can be observed that β_t is greater than that of Urea, whereas μ_t value of CMA is well above and those of FMA and BMA are comparable with that of Urea. Thus, the first order hyperpolarizability and total dipole moment value of the three molecules ascertain their non-linear optical character. Hence, the molecules FMA, CMA and BMA may be considered to develop further to demonstrate the second harmonic generation for non-linear effects for NLO applications in optoelectronics.

3.8. Thermodynamic parameters

Thermodynamic parameters can be obtained from the computed normal mode vibrational frequencies by adopting the principles of statistical mechanics. Using statistical thermodynamic calculations, the macroscopic quantities like heat capacities, entropies and enthalpies can be determined from the molecular energy levels which arise due to molecular translation, rotation, vibration and electronic excitation [72]. The thermodynamic parameters offer valuable information, like Entropy (S) that gives the direction of chemical reactions towards disorder, which determines the ability of a biomedical system to bind with its target [73]. They also help to develop the new schemes by considering the molecular interactions to explore the new drugs. To achieve the rotational and vibrational contribution to the partition function, the necessary structural parameters were taken from the results of DFT computations. Thus, the thermodynamic quantities like specific heat capacity at constant volume (C_v), entropy (S), SCF energy, vibrational energy (E_{vib}), zero-point energy (E_0) and rotational constants (A, B and C) of the test molecules were computed employing rigid rotator harmonic oscillator approximation using standard expressions [74,75] with DFT/ B3LYP/6-311++G(d,p) level of theory and are collected in Table 9. They facilitate the experimentalists to find the further related thermodynamic energies and the directions of chemical reactions using the relationships of thermodynamic functions and the second law of thermodynamics in thermo chemical field [76]. All the thermodynamic calculations were done in gas phase and pertain to one mole of perfect gas at one atm.

3.9. Natural bond orbital (NBO) analysis

The natural bond orbital (NBO) analysis gives the information on the structure of an optimized conformer in terms of localized bond and antibond orbitals; and Rydberg extra valence orbitals. It enables us to know the donor-acceptor interactions, electron delocalization, intra-molecular

Table 9
Thermodynamic parameters (for one mole of perfect gas at one atm) and rotational constants of FMA, CMA and BMA.

Thermodynamic parameters	Value		
	FMA	CMA	BMA
SCF Energy (in 10^3 kJ mol^{-1})	−1469.072	−2612.673	−7965.265
Total energy (thermal), E_{total} (kcal mol^{-1})	90.432	93.442	89.538
Heat capacity at const. volume, C_V (cal mol^{-1} K^{-1})	36.289	39.949	37.620
Heat capacity at const. pressure, C_P (cal mol^{-1} K^{-1})	38.275	41.935	39.606
Entropy, S (cal mol^{-1} K^{-1})	97.931	103.031	103.542
Vibrational energy, E_{vib} (kcal mol^{-1})	88.655	91.664	87.760
Zero-point vibrational energy, E_0 (kcal mol^{-1})	84.396	86.644	83.047
Rotational constants (MHz)			
A	1900.09	1288.23	1687.88
B	900.28	663.23	449.65
C	613.13	457.18	360.15

charge transfer and hydrogen bonding formation in the molecular systems. The natural bond orbitals are analyzed using the electron wave functions in terms of occupied Lewis-type (bond or lone pair) and unoccupied non-Lewis-type (anti-bond or Rydberg) localized orbitals [77, 78]. The electron delocalization (ED) in these orbitals results in stabilizing the donor-acceptor interactions. The stabilization energies of all the potential interactions can be determined using the second order perturbation theory. The interactions result in a loss of occupancy from the localized bond orbital of the idealized Lewis structure into an empty non-Lewis orbital. The delocalization effects are evaluated from the off-diagonal elements of the Fock matrix in the NBO basis employing DFT/B3LYP/6-311++G(d,p) level of computations using NBO 3.1 program [79] by implementing in the Gaussian 09 W software for FMA, CMA and BMA and are portrayed in Tables ST1-ST3 as supplementary information. The stabilization energy, E(2) resulted due to these delocalization interactions is estimated following the method proposed by Reed et al. [77].

The stabilization Energy $E(2)$ is evaluated using the equation given below [80].

$$E(2) = -q_i \frac{F_{ij}^2}{\Delta E} = -q_i \frac{\langle i|F|j\rangle^2}{\varepsilon_j - \varepsilon_i}$$

where q_i is the donor orbital occupancy, ε_i and ε_j are energies of ith and jth orbitals, respectively, and F_{ij} is the off diagonal NBO Fock matrix element.

Though, many stabilization energies are resulted due to various interactions, only some significant stabilization energy $E(2)$ values those are resulted due to strong interactions between the donors and acceptors of the conjugated molecular system are shown in Tables ST1–ST3. Intramolecular charge transfer takes place by hyper conjugative interactions those arise due to overlap between the bonding π-orbitals and antibonding π*-orbitals.

In FMA, the electron delocalization is maximum around bonding π orbitals of C1-C6, C2-C3 and C4-C5 bonds and is distributed to π* antibonding orbitals of C7-O13, C4-C5 and C1-C6 with stabilization energy of about 22.35, 21.71 and 21.80 kCal/ mol, respectively. The maximum stabilization energies 21.17, 19.19, 18.43 and 20.52 kCal/ mol are resulted due to π → π*electron transition about C2-C3, C4-C5, C1-C6 and C2-C3, respectively. The maximum stabilization energies for lone pair electrons of LP(2)O14 and LP(3)F9 → π* (C7-O13 and C2-C3) are found as 41.99 and 16.76 kCal/mol, respectively. The σ → σ* transition occurs with stabilization energy of about 16.97, 33.30 and 6.11 kCal/mol, respectively due to the bonding of lone pair electrons of LP(2)O13 and LP(1)O14 to σ* anti-bonding of (C1-C7 and C7-O14) and C7-O13.

In CMA, maximum π-electron delocalization occurs between C1-C2, C3-C4 and C5-C6 bonding orbitals and π* anti-bonding orbitals of C5-C6, C1-C2 and C3-C4 with stabilization energy at 19.27, 21.52 and 24.78 kCal/ mol, respectively. The maximum stabilization energies 18.27, 15.89 and 20.22 kCal/ mol are due to π → π*electron transition between the π bonding orbitals of C1-C2, C3-C4 and C5-C6 bonds and π* antibonding orbitals of C3-C4, C5-C6 and C1-C2, respectively. The maximum stabilization energies due to interaction between the lone pair electrons of LP(2)O14 and LP(3)C19 bonds and π* anti-bonding orbitals of [(C7-O13) and (C3-C4)] are found as 46.58 and 12.05 kCal/mol, respectively. The σ electron delocalization is maximum around the lone pair electrons of LP(2)O13 and LP(1)O14 which are distributed to σ* anti-bonding of (C1-C7 and C7-O14) and C7-O13 with stabilization energy of about 19.50, 33.89 and 5.60 kCal/mol, respectively.

In BMA, the π electron delocalization is maximum around C1-C6 and C4-C5 that is distributed to π* anti-bonding of C2-C3 and C1-C6 with stabilization energy of about 23.45 and 23.08 kCal/ mol, respectively. The maximum stabilization energies 21.92, 19.13, 18.50, 18.26, and 16.38 kCal/ mol are due to the π electron delocalization about C2-C3, C4-C5,C1-C6 and C2-C3 that is distributed to π* anti-bonding of C4-C5, C2-C3,C7-O13, C4-C5 and C1-C6, respectively. Maximum σ electron delocalization occurs around C1-C2 and C4-C5 due to σ* antibonding of C3-Br9 and C3-Br9 with stabilization energy of about 5.78 and 5.17 kCal/mol, respectively. The electron transition between the lone pair electrons of LP(2)O13 to σ*(C7-O13) and σ*(C1-C7) results with stabilization energy of 33.09 and 17.53 kCal/mol. The lone pair of LP(2)O14 and LP(3)Br9 and π* anti-bonding orbitals of (C7-C13) and (C2-C3) transitions takes place with stabilization energy of 42.24 and 9.18 kcal/mol, respectively.

The results of NBO and MEP surface analyses show that the maximum electrophilic potential atoms are giving the electrons to the nearby acceptors.

4. Conclusion

Using experimental and DFT/B3LYP/6-311++G(d,p) approaches, the comprehensive spectroscopic analyses on 3-fluoro-2-methylbenzoic acid (FMA); 3-chloro-2-methoxybenzoic acid (CMA); and 3-bromo-2-methylbenzoic have been quantified. The optimized molecular geometry reveals that the computed structure parameters are closely associated with the experimental literature values of related molecules. The spectral analyses were made unambiguously for vibrational assignments of fundamental frequencies using PED. The electronegative effect of the surrounding atoms of the molecules was studied by detected and simulated ^{1}H and ^{13}C NMR chemical shifts. Examining the small energy gap between HOMO and LUMO and computed global reactivity descriptors reveal their chemical reactivity and stability. The simulated absorption maxima of the three molecules at TD-DFT/B3LYP/6-311++G(d,p) level demonstrated better agreement with their detected counterparts in DMSO-d_6 solvent using IEF-PCM solution model. A pair of absorption maxima observed in each of the three molecules was attributed due to n → π*; and π → π* transitions associated with H → L; and H-1 → L, H-2 → L and H-3 → L interactions, respectively. According to the MEP plot, the oxygen atom contains nucleophilic site in three molecules, whereas the hydrogen atom of acid group moiety in FMA and BMA; and the fluorine atom and methyl group in CMA consist electrophilic regions. The computed NLO parameters μ_t and β_t of the test molecules revealed on comparison with associated threshold values of Urea that they are good for developing NLO materials for opto-electronic industry. NBO analysis exhibited the electron delocalization due to intra-molecular interaction between the acceptor and donor atoms to offer stabilization of the molecules. Thermodynamic functions and rotational constants were also evaluated using the same level of theory for these molecules, which may facilitate the pharmacists to know the directions of chemical reactions and to develop novel strategies for the invention of new drugs.

CRediT authorship contribution statement

Sreenivas Boda: Conceptualization, Investigation. **L. Ravindranath:** Methodology, Resources. **K. Srishailam:** Software, Data curation. **G. Ramesh:** Formal analysis. **Jai Kishan Ojha:** Writing – original draft. **B. Venkatram Reddy:** Formal analysis, Writing – review & editing.

Declaration of Competing Interest

The authors declare that they have no known competing financial interests or personal relationships that could have appeared to influence the work reported in this paper

Data availability

No data was used for the research described in the article.

Acknowledgements

The authors express their gratitude to the Sophisticated Analytical Instrumentation Facility (SAIF), IIT Madras, Chennai, India, for spectral measurements. The first author (Sreenivas Boda) and corresponding author sincerely acknowledges the Department of Physics for having provided chemicals from UGC-SAP DRS-II project (No. F. 530/24/DRS-II/2015 (SAP-I), dated 08-05-2018) for executing this research work. The remaining authors thank the managements of their respective affiliations for having facilitated to carry out this research.

Supplementary materials

Supplementary material associated with this article can be found, in the online version, at doi:10.1016/j.molstruc.2023.137078.

References

[1] N. Sundaraganesan, S. Illakiamni, B.D. Joshua, FT-Raman and FT-IR spectra, ab initio and density functional studies of 2-amino-4,5-difluorobenzoic acid, Spectrochim. Acta A 67 (2) (2007) 287–297, https://doi.org/10.1016/j.saa.2006.07.016.

[2] M.A. Palafox, M. Gil, J.L. Nunez, Structure and spectral characteristics of o-aminobenzoic acid by AM1, Vib. Spectrosc. 6 (1) (1993) 95–105, https://doi.org/10.1016/0924-2031(93)87026-P.

[3] R. Swinslocka, M. Samsonowicz, E. Regulaska, W. Lewandowski, Molecular structure of 4-aminobenzoic acid salts with alkali metals, J. Mol. Struct. 792 (2006) 227–238, https://doi.org/10.1016/j.molstruc.2005.10.060.

[4] N. Sundaraganesn, B. Anand, C. Megnathn, B.D. Joshua, FT-IR, FT-Raman spectra and ab initio HF, DFT vibrational analysis of *p*-chlorobenzoic acid, Spectrochim. Acta A 69 (2008) 871–879, https://doi.org/10.1016/j.saa.2007.05.051.

[5] S. Kanchan, D.N.S. Jayachandra, Effect of *Parthenium hysterophorus* on nitrogen-fixing and nitrifying bacteria, Can. J. Bot. 59 (2) (1981), https://doi.org/10.1139/b81-030.

[6] J.F. Lynas, B. Walker, Bioorg, Peptide argininol "inverse substrates" of anisic acid: novel inhibitors of the trypsin-like serine proteinases, Med. Chem. Lett. 7 (1997) 1133–1138, https://doi.org/10.1016/S0960-894X(97)00174-1.

[7] M. Samsonowicks, T. Hrynaszkiewicz, R.S. Wislocka, E. Regulska, W. Lewandowski, Experimental and theoretical IR, Raman, NMR spectra of 2-, 3- and 4-aminobenzoic acids, J. Mol. Struct. 345 (2005) 744–752, https://doi.org/10.1016/j.molstruc.2004.11.063.

[8] M. Chapman, P.K. Verma, Laser Raman and FTIR spectra of 2,3,5-tri-iodobenzoic acid, Ind. J. Phys. 77B (2003) 315–318. http://hdl.handle.net/10821/6762.

[9] N. Sundaraganesan, B.D. Joshua, T. Rajdakoumar, Molecular structure and vibrational spectra of 2-chlorobenzoic acid by density functional theory and ab-initio Hartree–Fock calculations, Ind. J. Pure Appl. Phys. 47 (2009) 248–258. http://nopr.niscpr.res.in/handle/123456789/4075.

[10] C. Meganathan, S. Sebastian, M. Kurt, K.W. Lee, N. Sundaraganesan, Molecular structure, spectroscopic (FTIR, FTIR gas phase, FT-Raman) first-order hyperpolarizability and HOMO–LUMO analysis of 4-methoxy-2-methyl benzoic acid, J. Raman Spectrosc. 41 (2010) 1369–1378, https://doi.org/10.1002/jrs.2562.

[11] Y. Gu, W. Yang, A. Hao, Q. Xu, Y. Hu, Determination and analysis of solubility of 3-bromo-2-methylbenzoic acid in different solvent systems at different temperatures, J. Chem. Eng. Data 65 (4) (2020) 1571–1582, https://doi.org/10.1021/acs.jced.9b01007.

[12] A.S. Batsanov, 3-fluoro-4-methylbenzoic acid, Acta Cryst. E60 (2004) 01948–01949, https://doi.org/10.1107/S1600536804024389.

[13] G. Ramesh, B.V. Reddy, Barrier potential, structure (monomer & dimer), inter- & intra- molecular interactions, vibrational analysis, Fukui functions, MESP, NBO, UV and NMR analysis of pyridine-3-carboxylic acid using spectroscopic and DFT approach, Polycycl. Aromat. Compd. 43 (3) (2023) 2488–2505, https://doi.org/10.1080/10406638.2022.2046614.

[14] J. Prashanth, K. Ramaiah, B.V. Reddy, Barrier potentials, molecular structure, force filed calculations and quantum chemical studies of some bipyridine di-carboxylic acids using the experimental and theoretical using (DFT, IVP) approach, Mol. Simul. 45 (2019) 1353–1383, https://doi.org/10.1080/08927022.2019.1634807.

[15] J. Prashanth, J.K. Ojha, B.V. Reddy, G.R. Rao, Experimental and theoretical study of 3-methyl-4-nitrobenzoic acid using DFT and IVP methods, J. Phys.: Conf. Ser. 759 (2016), 012057, https://doi.org/10.1088/1742-6596/759/1/012057.

[16] J. Laxman Naik, B. Venkatram Reddy, N. Prabavathi, Experimental (FTIR and FT-Raman) and theoretical investigation of some pyridine-dicarboxylic acids, J. Mol. Struct. 1100 (2015) 43–58, https://doi.org/10.1016/j.molstruc.2015.06.064.

[17] N. Prabavathi, N. Senthil Nayaki, B. Venkatram Reddy, Molecular structure, vibrational spectra, natural bond orbital and thermo dynamic analysis of 3,6-dichloro-4-methylpyridazine and 3,6- dichloropyridazine-4-carboxylic acid by dft approach, Spectrochim. Acta A 136 (2015) 1134–1148, https://doi.org/10.1016/j.saa.2014.09.137.

[18] J. Prashanth, G. Ramesh, J.L. Naik, J.K. Ojha, B.V. Reddy, G.R. Rao, Molecular structure, vibrational analysis and first order hyperpolarizability of 4-methyl-3-nitrobenzoic acid using density functional theory, Opt. Photonics J. 5 (2015) 91–107, https://doi.org/10.4236/opj.2015.53008.

[19] S. Pramanik, T. Dey, A.K. Mukherjee, Five benzoic acid derivatives: crystallographic study using X-ray powder diffraction, electronic structure and molecular electrostatic potential calculation, J. Mol. Struct. 1175 (2019) 185–194, https://doi.org/10.1016/j.molstruc.2018.07.090.

[20] Q.Z. Liu, S.S. Wang, T.F. Wang, et al., Experimental and theoretical studies on a novel helical architecture driven by hydrogen and halogen bonding interactions, J. Chem. Sci. 128 (2016) 1895–1904, https://doi.org/10.1007/s12039-016-1195-9.

[21] A.D. Becke, A new mixing of Hartree–Fock and local density-functional theories, J. Chem. Phys. 98 (1993) 1372–1377, 10.1063/1.464304.

[22] C. Lee, W. Yang, R.G. Parr, Development of the Colle–Salvetti correlation-energy formula into a functional of the electron density, Phys. Rev. B 37 (1988) 785–789, https://doi.org/10.1103/PhysRevB.37.785.

[23] M.J. Frisch, G.W. Trucks, H.B. Schlegel, G.E. Scuseria, M.A. Robb, J.R. Cheeseman, G. Scalmani, V. Barone, B. Mennucci, G.A. Petersson, et al., Gaussian, Inc., Wallingford CT, 2010.

[24] R. Dennington et al., Gauss View, Version 5.0, Semichem Inc, Shawnee Mission, 2009.

[25] G. Fogarasi, X. Zhou, P.W. Tayler, P. Pulay, The calculation of ab initio molecular geometries: efficient optimization by natural internal coordinates and empirical correction by offset forces, J. Am. Chem. Soc. 14 (1992) 8191–8201, https://doi.org/10.1021/ja00047a032.

[26] P. Pulay, G. Fogarasi, G. Pongor, J.E. Boggs, A. Vargh, Combination of theoretical ab initio and experimental information to obtain reliable harmonic force constants. Scaled quantum mechanical (QM) force fields for glyoxal, acrolein, butadiene, formaldehyde, and ethylene, J. Am. Chem. Soc. 105 (24) (1983) 7037–7047, https://doi.org/10.1021/ja00362a005.

[27] T. Sundius, MOLVIB—A flexible program for force field calculations, J. Mol. Struct. 218 (1990) 321–326, https://doi.org/10.1016/0022-2860(90)80287-T.

[28] T. Sundius, Scaling of ab initio force fields by MOLVIB, Vib. Spectrosc. 29 (2002) 89–95, https://doi.org/10.1016/S0924-2031(01)00189-8.

[29] Z. Latajka, W.B. Person, K. Morokuma, An ab initio calculation of the infrared spectrum and tautomerism of guanine, J. Mol. Struct. Theochem. 135 (1986) 253–266, https://doi.org/10.1016/0166-1280(86)80063-X.

[30] G. Keresztury, S. Holly, G. Besenyei, J. Varga, A. Wang, J.R. Durig, Vibrational spectra of monothiocarbamates-II. IR and Raman spectra, vibrational assignment, conformational analysis and ab initio calculations of *S*-methyl-*N,N*-dimethylthiocarbamate, Spectrochim Acta A 49 (13–14) (1993), https://doi.org/10.1016/S0584-8539(09)91012-1, 2007–2017, 2019–2026.

[31] G. Kereztury, et al., Raman Spectroscopy: Theory in Handbook of Vibrational Spectroscopy, 1, John Wiley and Sons Ltd., New York, 2002, pp. 71–87.

[32] K. Wolinski, R. Haacke, J.F. Hinton, P. Pulay, Methods for parallel computation of SCF NMR chemical shifts by GIAO method: efficient integral calculation, multi-Fock algorithm, and pseudodiagonalization, J. Comput. Chem. 18 (6) (1997) 816–825, 10.1002/(SICI)1096-987X(19970430)18:6<816::AID-JCC7>3.0.CO;2-V.

[33] E. Runge, E.K.U. Gross, Density-functional theory for time-dependent systems, Phys. Rev. Lett. 52 (1984) 997–1000, https://doi.org/10.1103/PhysRevLett.52.997.

[34] G. Scalmani, M.J. Frisch, Continuous surface charge polarizable continuum models of solvation. I. General formalism, J. Chem. Phys. 132 (2010), 114110, https://doi.org/10.1063/1.3359469.

[35] A.D. Buckingham, J.O. Hirchfelder (Eds.), Advances in Chemical Physics, Wiley Online Library, 1967, https://doi.org/10.1002/9780470143582.ch2.

[36] A.E.L. Reed, L.A. Curtiss, F. Weinhold, Intermolecular interactions from a natural bond orbital, donor-acceptor viewpoint, Chem. Rev. 88 (1988) 899–926, https://doi.org/10.1021/cr00088a005.

[37] E. Bright Wilson Jr., The normal modes and frequencies of vibration of the regular plane hexagon model of the benzene molecule, Phys. Rev. 45 (1934) 706–714, https://doi.org/10.1103/PhysRev.45.706.

[38] B.V. Reddy, G.R. Rao, Transferable valence force fields for substituted benzens—Part I. Monohalogenated anisoles, Vib. Spectrosc. 6 (1994) 231–250, https://doi.org/10.1016/0924-2031(93)E0056-8.

[39] J.K. Ojha, B.V. Reddy, G. Ramana Rao, Vibrational analysis and valence force field for nitrotoluenes, dimethylanilines and some substituted methylbenzenes, Spectrochim. Acta Part A 96 (2012) 632–643, https://doi.org/10.1016/j.saa.2012.06.035.

[40] M. Karabacak, E. Kose, M. Kurt, FT-Raman, FT-IR spectra and DFT calculations on monomeric and dimeric structures of 5-fluoro- and 5-chloro-salicyclic acid, J. Raman Spectrosc. 41 (2010) 1085–1097, https://doi.org/10.1002/jrs/.2551.

[41] D.R. Leenaraj, D. Manimaran, J.I. Hubert, Molecular docking and structural analysis of non-opioid analgesic drug acemetacin with halogen substitution: a DFT approach, J. Mol. Struct. 1123 (2016) 180–190, https://doi.org/10.1016/j.molstruc.2016.06.035.

[42] J. Prashanth, K. Ramaiah, B.V. Reddy, Barrier potentials, molecular structure, force filed calculations and quantum chemical studies of some bipyridine di-carboxylic acids using the experimental and theoretical using (DFT, IVP) Approach, Mol. Simul. 45 (16) (2019) 1353–1383, https://doi.org/10.1080/08927022.2019.1634807.

[43] G. Ramesh, B.V. Reddy, Spectroscopic investigation on structure (monomer and dimer), molecular characteristics and comparative study on vibrational analysis of picolinic and isonicotinic acids using experimental and theoretical (DFT & IVP) methods, J. Mol. Struct. 1160 (2018) 271–292, https://doi.org/10.1016/j.molstruc.2018.01.083.

[44] H. Malarkodi, et al., Molecular structure, spectral, electronic and thermodynamic, first-order hyperpolarizability, NBO and molecular docking studies of novel acenaphthylene pyrrolidine derivative, Chem. Select 3 (2018) 11552–11564, https://doi.org/10.1002/slct.201802535.
[45] S. Sebastian, N. Sundaraganesan, The spectroscopic (FT-IR, FT-IR gasphase, FT-Raman and UV) and NBO analysis of 4-Hydroxypiperidine by density functional method, Spectrochim. Acta A 75 (2010) 941–952, https://doi.org/10.1016/j.saa.2009.11.030.
[46] J. Chocholousova, V.V. Spirko, P. Hobza, First local minimum of the formic acid dimer exhibits simultaneously red-shifted O–H···O and improper blue-shifted C–H···O hydrogen bonds, Phys. Chem. Chem. Phys. 6 (2004) 37–41, https://doi.org/10.1039/B314148A.
[47] R.M. Parrish, E.G. Hohenstein, P.L. McMahon, T.J. Martínez, Quantum computation of electronic transitions using a variational quantum eigensolver, Phys. Rev. Lett. 122 (2019), 230401, https://doi.org/10.1103/PhysRevLett.122.230401.
[48] D. Jacquemin, E.A. Perpete, I. Ciofini, C. Adamo, Accurate simulation of optical properties in dyes, Acc. Chem. Res. 42 (2) (2009) 326–334, https://doi.org/10.1021/ar800163d.
[49] D. Jacquemin, J. Preat, V. Wathelet, M. Fontaine, E.A. Perpète, Thioindigo dyes: highly accurate visible spectra with TD-DFT, J. Am. Chem. Soc. 128 (6) (2006) 2072–2083, https://doi.org/10.1021/ja056676h.
[50] I. Ciofini, C. Adamo, Accurate evaluation of valence and low-lying rydberg states with standard time-dependent density functional theory, J. Phys. Chem. A 111 (25) (2007) 5549–5555, https://doi.org/10.1021/jp0722152.
[51] D. Maric, J.P. Burrows, Application of a gaussian distribution function to describe molecular UV−vis. absorption continua. 1. Theory, J. Phys. Chem. A 100 (21) (1996) 8645–8659, https://doi.org/10.1021/jp952548b.
[52] D. Maric, J.N. Crowley, J.P. Burrows, Application of a Gaussian distribution function to describe molecular UV−visible absorption continua. 2. The UV spectra of $RO_2^{\bullet}$ radicals, J. Phys. Chem. A 101 (14) (1997) 2561–2567, https://doi.org/10.1021/jp961715k.
[53] E.A.G. Bremond, J. Kieffer, C.J. Adamo, A reliable method for fitting TD-DFT transitions to experimental UV–visible spectra, J. Mol. Struct. 954 (1–3) (2010) 52–56, https://doi.org/10.1016/j.theochem.2010.04.038.
[54] D. Jacquemin, E.A. Perpète, Ab initio calculations of the colour of closed-ring diarylethenes: TD-DFT estimates for molecular switches, Chem. Phys. Lett. 429 (1–3) (2006) 147–152, https://doi.org/10.1016/j.cplett.2006.08.028.
[55] J. Preat, C. Michaux, A. Lewalle, E.A. Perpète, D. Jacquemin, Delocalisation in conjugated triazene chromophores: insights from theory, Chem. Phys. Lett. 451 (1–3) (2008) 37–42, https://doi.org/10.1016/j.cplett.2007.11.056.
[56] G. Scalmani, M.J. Frisch, Continuous surface charge polarizable continuum models of solvation. I. General formalism, J. Chem. Phys. 132 (2010), 114110, https://doi.org/10.1063/1.3359469.
[57] K. Fukui, Role of frontier orbitals in chemical reactions, Science 218 (1982) 747–754, https://doi.org/10.1126/science.218.4574.747.
[58] T.A. Koopmans, Ordering of wave functions and eigen energies of the individual electrons of an atom, Physica 1 (1993) 104–113, https://doi.org/10.1016/S0031-8914(34)90011-2.
[59] C.H. Choi, M. Kertesz, Conformational information from vibrational spectra of styrene, trans-stilbene, and cis-stilbene, J. Phys. Chem. A 101 (1997) 3823–3831, https://doi.org/10.1021/jp970620v.
[60] S. Leena, O. Prasad, V.N. Mishra, S.R. Shukla, Raman, FT-IR spectroscopic analysis and first-order hyperpolarisability of 3-benzoyl-5-chlorouracil by first principles, J. Mol. Simul. 37 (2011) 153–163, https://doi.org/10.1080/08927022.2010.533273.
[61] D.F.V. Lewis, C. Ioannides, D.V. Parke, Interaction of a series of nitriles with the alcohol-inducible isoform of P450: computer analysis of structure-activity relationships, Xenobiotica 24 (1994) 401–408, https://doi.org/10.3109/00498259409043243.
[62] D. Kosar, C. Albayrak, Spectroscopic investigations and quantum chemical computational study of (E)-4-methoxy-2-[(p-tolylimino)methyl]phenol, Spectrochim. Acta A 78 (2011) 160–167, https://doi.org/10.1016/j.saa.2010.09.016.
[63] C. Parlak, Ö. Alver, O. Baglayan, P. Ramasami, Theoretical insights of the drug-drug interaction between favipiravir and ibuprofen: a DFT, QTAIM and drug-likeness investigation, J. Biomol. Struct. Dyn. 41 (10) (2023) 4313–4320, https://doi.org/10.1080/07391102.2022.2066022.
[64] G.P. Sheeja Mol, D. Aruldhas, I.H. Joe, Chemical reactivity, molecular electrostatic potential and in-silico analysis on benzimidazole fungicide benomyl, Heliyon 8 (2022) e11417, https://doi.org/10.1016/j.heliyon.2022.e11417.
[65] K. Vedhapriya, et al., Quantum computational, molecular structure interaction, bonding, spectral and hiershfeld surface analysis of -2-deoxy-2-[[(methylnitrosoamino)carbonyl] amino]-D-glucose-anti-hematologic cancer agent, Chem. Phys. Impact 7 (2023) 100262–100279, https://doi.org/10.1016/j.chphi.2023.100262.
[66] Y.-X. Sun, Q.-L. Hao, W.-X. Wei, Z.-X. Yu, L.-D. Lu, X. Wang, Y.-S. Wang, Experimental and density functional studies on 4-(3,4-dihydroxybenzylideneamino)antipyrine,and 4-(2,3,4-trihydroxybenzylideneamino)antipyrine, J. Mol. Struct. 904 (1–3) (2009) 74–82, https://doi.org/10.1016/j.theochem.2009.02.036.
[67] Y.X. Sun, Q.L. Hao, W.X. Wei, Z.X. Yu, L.D. Lu, X. Wang, Y.S. Wang, Experimental and density functional studies on 4-(4-cyanobenzylideneamino)antipyrine, Mol. Phys. 107 (2009) 223–235, https://doi.org/10.1080/00268970902769471.
[68] C. Andraud, T. Brotin, C. Garcia, F. Pelle, P. Goldner, B. Bigot, A. Collet, Theoretical and experimental investigations of the nonlinear optical properties of vanillin, polyenovanillin, and bisvanillin derivatives, J. Am. Chem. Soc. 116 (5) (1994) 2094–2102, https://doi.org/10.1021/ja00084a055.
[69] N. Subramanian, N. Sundaraganesan, J. Jayabharathi, Spectroscopic (FT-IR, FT-Raman, NMR, UV) studies and first-order molecular hyperpolarizabilities of 1,2-bis (3-methoxy-4-hydroxybenzylidene)hydrazine by density functional method, Spectrochim. Acta A 76 (2010) 259–269, https://doi.org/10.1016/j.saa.2010.03.033.
[70] H.S. Nalwa, S. Miyata, Nonlinear Optics of Organic Molecules and Polymers, CRC Press, Boca Raton, 1997.
[71] K.S. Pitzer, Molecular Structure and Statistical Thermodynamics, World Scientific Series in 20th Century Chemistry, World Scientific 1 (1993), https://doi.org/10.1142/2063.
[72] C.S. Abraham, et al., Quantum computational studies, spectroscopic (FT-IR, FT-Raman and UV–vis) profiling. Natural hybrid orbital and molecular docking analysis on 2,4 dibromoaniline, J. Mol. Struct. 1160 (2018) 393–405, https://doi.org/10.1016/j.mostruc.2018.02.022.
[73] S. Janani, H. Rajagopal, S. Muthu, S. Aayisha, M. Raja, Molecular structure, spectroscopic (FT-IR, FT-Raman, NMR), HOMO-LUMO, chemical reactivity, AIM, ELF, LOL and Molecular docking studies on 1-benzyl-4-(N-Boc-amino)piperidine, J. Mol. Struct. 1230 (2021), 129657, https://doi.org/10.1016/j.molstruc.2020.129657.
[74] G. Herzberg, Infrared and Raman Spectra of Polyatomic Molecules, D. Van Nostrand, New York, 1945.
[75] K.S. Pitzer, W.D. Gwinn, Energy levels and thermodynamic functions for molecules with internal rotation I. Rigid frame with attached tops, J. Chem. Phys. 10 (1942) 428–440, https://doi.org/10.1063/1.1723744.
[76] L. Sinha, M. Karabacak, V. Narayana, M. Cinar, O. Prasad, Molecular structure, electronic properties, NLO, NBO analysis and spectroscopic characterization of Gabapentin with experimental (FT-IR and FT-Raman) techniques and quantum chemical calculations, Spectrochim. Acta A 109 (2013) 298–307, https://doi.org/10.1016/j.saa.2013.02.035.
[77] A.E. Reed, L.A. Curtiss, F. Weinhold, Intermolecular Interactions from a natural bond orbital, donor-acceptor viewpoint, Chem. Rev. 88 (6) (1988) 899–926, https://doi.org/10.1021/cr00088a005.
[78] J.P. Foster, F. Weinhold, Natural hybrid orbitals, J. Am. Chem. Soc. 102 (1980) 7211–7218, https://doi.org/10.1021/ja00544a007.
[79] E.D. Glendening, A.E. Reed, J.E. Carpenter, and F. Weinhold, NBO Version 3. 1 (University of Wisconsin, Madison: TCI, 1998).
[80] P. Politzer, J.S. Murray, The fundamental nature and role of the electrostatic potential in atoms and molecules, Theor. Chem. Acc. 108 (2002) 134–142, https://doi.org/10.1007/s00214-002-0363-9.